Attributing trend in naturalized streamflow to temporally explicit vegetation change and climate variation in the Yellow River Basin of China

Zhihui Wang[1,3], Qiuhong Tang[2], Daoxi Wang[1,3], Peiqing Xiao[1], Runliang Xia[4], Pengcheng Sun[1], Feng Feng[5]

[1]Key Laboratory of Soil and Water Conservation on the Loess Plateau of Ministry of Water Resources, Yellow River Institute of Hydraulic Research, Yellow River Conservancy Commission, Zhengzhou, 450003, China
[2]Key Laboratory of Water Cycle and Related Land Surface Processes, Institute of Geographic Sciences and Natural Resources Research, Chinese Academy of Sciences, Beijing, 100101, China
[3]Henan Key Laboratory of Ecological Environment Protection and Restoration of the Yellow River Basin, Yellow River Institute of Hydraulic Research, Zhengzhou, 45003, China
[4]Henan Engineering Research Center of Smart Water Conservancy, Yellow River Institute of Hydraulic Research, Zhengzhou, 45003, China
[5]Yellow River Conservancy Technical Institute, Kaifeng, 475004, China

Correspondence to: Qiuhong Tang (tangqh@igsnrr.ac.cn)

Abstract. The naturalized streamflow, i.e., streamflow without water management effects, in the Yellow River Basin (YRB) has been significantly decreased at a rate of -3.71×10^8 m^3·yr^{-1} during 1982-2018 although annual precipitation experienced insignificantly positive trend. Explicit detection and attribution of naturalized streamflow is critical to manage limited water resources for sustainable development of ecosystem and socio-economical system. The effects from temporally explicit changes of climate variables and underlying surfaces on the streamflow trend were assessed using Variable Infiltration Capacity (VIC) model prescribed with continuously dynamic leaf area index (LAI) and land cover. The results show a sharp increase of LAI trend and land use change as a conversion of cropland into forest-grass in the basin. The decrease in naturalized streamflow can be primarily attributed to the vegetation changes including interannual LAI increase and intra-annual LAI temporal pattern change, which accounts for the streamflow reduction of 1.99×10^8 m^3·yr^{-1} and 0.45×10^8 m^3·yr^{-1}, respectively. The impacts of LAI change are largest at the sub-region of Longmen-Huayuankou where LAI increasing trend is high and land use change is substantial. Attribution based on simulations with multi-year average LAI changes obviously underestimates the impacts of interannual LAI change and intra-annual LAI temporal change on the natural streamflow trend. Overall, the effect of climate variation on streamflow is slight because positive effect from precipitation and wind speed changes was offset by the negative effect from increasing temperature. Although climate variation is decisive for streamflow change, this study suggests that change in underlying surface has imposed a substantial trend on naturalized streamflow. This study improves the understanding of the spatiotemporal patterns and the underlying mechanisms of natural streamflow reduction across YRB between 1982 and 2018.

1 Introduction

35 The Yellow River is the second-longest river in China and its contribution to Chinese civilisation has earned it the title of the country's "Mother River". It originates in the Tibetan Plateau, flows through the Loess Plateau and North China Plain, and discharges into the Bohai Gulf, and it has a total length of about 5,464 km and drains a watershed of 752,443 km^2 (Tang et al., 2013). It supports 30% of China's population and 13% of China's total cultivated area with water resources accounting for only about 2.6% of China's water (Cuo et al., 2013). Because of less precipitation, there is a critical water shortage

40 problem in the Yellow River Basin (YRB). The basin has only 620 m^3 in per capita water resources, which is 30% and 7.5% of the national and global per capita water resources, respectively (Fu et al., 2004; Bao et al., 2019).

Like elsewhere throughout the world, climate change is taking place in the YRB as reported by previous studies (Fu et al., 2004; Xu et al., 2007; Hu et al., 2011). These studies consistently reported temperature increases, spatio-temporal variations in precipitation in the YRB. Meanwhile, to mitigate the severe soil erosion and deteriorating ecological environment, a series

45 of soil and water conservation measures and ecological restoration projects have been implemented by Chinese government, including afforestation, Grain for Green Project (GFGP), grazing prohibition, terraces, and check dams (Yao et al., 2011; Jia et al., 2014). In recent three decades, the YRB has experienced drastic change of underlying surface conditions, including land use/cover, vegetation structure, topography and frozen soil, which has significantly altered the evapotranspiration and terrestrial water storage associated with runoff and its routing processes (Cheng and Jin, 2013; Sun et al., 2015; Bai et al,

50 2019; Yang et al., 2020; Zhai et al., 2021; Wang et al., 2022). A number of observational studies have shown that streamflow in different parts (e.g., source region, Loess Plateau, etc.) of the YRB decreased over the past decades (Tang et al., 2008; Hu et al., 2011; Zhao et al., 2015; Feng et al., 2016; Wu et al., 2018). This may lead to more serious water use conflict between ecosystem and socio-economical system. With the increasing scarcity of water resources, ecologists, hydrologists and decision makers have paid considerable attention to how much of the observed change in annual streamflow of YRB can be

55 attributed to climate variability and human activities for adaption in future water resources management (Chang et al., 2016; Wu et al., 2018).

Numerous studies have been conducted to investigate the change in river streamflow induced by climate change and human activities under global change (Tang, 2020). Statistical method including double mass curve (Gao et al., 2011) and climate elasticity model (Roderick et al., 2011) was the easy-to-use way to identify the contributions of climate and human

60 impacts on runoff, whereas it lacks the physical mechanism description and only can assess the overall impact induced by human activities. As the first analytical expression of Budyko's hypothesis was proposed by Fu (1981) according to the hydrological and climatic physical mechanism of the basin, Budyko-based elasticity method have been extensively used in the YRB to quantify the influence of changes in precipitation, potential evapotranspiration and watershed natural features on streamflow (Zhang et al., 2008; Zhao et al., 2014). To further isolate the vegetation effect on the streamflow, the relationship

65 between watershed feature parameter and vegetation change at catchment scale has been detailed discussed in different

basins and regions in the YRB (Zhang et al., 2016; Bao et al., 2019, Wang et al., 2021). However, above methodology is only able to attribute the multi-year average streamflow change between different periods.

Recently, process-based hydrological models have been used more and more widely due to interannual change of climate variables, vegetation, irrigation, dams and coal mining, etc. can be considered in the model to some extent for quantifying the impacts of various factors on the hydrological process (Tang et al., 2008; Tang et al., 2013; Wang et al., 2017; Luan et al., 2020). Very few studies focused on the impact of intra-annual temporal pattern change of climate variables and vegetation on the streamflow (Tang et al., 2008). Among commonly used models, the variable infiltration capacity (VIC) model is a physically-based macroscale hydrological model developed to solve water and energy balances (Liang et al., 1994, 1996). It has been successfully applied to simulate and attribute natural hydrological processes at both regional and global scales (Matheussen et al., 2000; Haddeland et al., 2006; Xie et al., 2007; Wang et al., 2012; Zhang et al., 2014; Yuan et al., 2016; Zhai et al., 2018; Yao et al., 2019; Zhu et al., 2021). The VIC model is usually run with static land cover and climatological vegetation leaf area index (LAI) throughout the simulation period as a result of specific model configuration (Wang et al., 2012; Xie et al., 2015). Previous studies have confirmed that the simulation accuracies of VIC model have been obviously improved in the intra-annual dynamics of soil moisture (Ford & Quiring, 2013), evapotranspiration (Tang et al, 2012) and runoff (Zhai et al., 2021) when remotely sensed intra-annual LAI dynamics instead of constant climatological LAI were used as input data during simulation process. However, vegetation phenological dynamics and LAI can show a large interannual variation (Wu et al., 2016; Piao et al., 2019), and VIC simulations considering year-to-year variability of LAI are able to better capture the interannual variation of runoff (Tesemma et al., 2015). Therefore, traditional configuration in land cover and vegetation parameters of VIC model probably underestimate the cumulative contribution of interannual vegetation change to the hydrological cycle (Xie et al., 2015). Improvement of the VIC model by coupling yearly land cover and continuously dynamic vegetation parameters that can be retrieved from remote sensing data sets would be favorable to remedy this issue (Tang et al., 2008, Xie et al., 2015; Yang et al, 2019).

Table 1 summarizes some typical studies about the attribution of annual runoff change in YRB and in China. Apparently, the inconsistencies between these studies stem from the different methods, time periods, and base scenarios used. None of these studies examined the influence of the temporally explicit vegetation change and climate variation on natural streamflow trend across the YRB. The specific objectives of this paper include to: 1) develop a VIC simulation scheme which enables VIC to reflect the cumulative effect of dynamic vegetation on the hydrological cycle by coupling time-series land cover and LAI remote sensing data; 2) assess the impacts of interannual change and intra-annual temporal pattern change of climatic factors, interannual change and intra-annual temporal pattern change of vegetation, and their interactive effect on the streamflow trend of YRB during 1982-2018; 3) compare the difference in attribution of streamflow change using VIC with and without considering continuous dynamics of LAI, and analyse the underlying causes of effects of different influencing factors on streamflow reduction.

Table 1. Summarizing typical studies carried out in the YRB and China for attributing interannual streamflow change

Study	Region	Method	Purpose

Tang et al. (2008)	Yellow River Basin	Distributed biosphere hydrological (DBH) model	Assessing the impacts of interannual change and temporal pattern change of climatic factors, interannual vegetation change on the change trend of interannual streamflow during 1960-2000.
Gao et al. (2011)	The middle reaches of the Yellow River	Double mass curve	Separating the impacts of precipitation and human activities on the multi-year average change of streamflow between 1950-1985 and 1985-2008.
Tang et al. (2013)	Yellow River Basin	Soil and water assessment tool (SWAT)	Estimating the impacts of interannual change of climatic factors on the multi-year average change of streamflow between 1960-1990 and 2003-2011.
Cuo et al. (2013)	The source region of the Yellow River	Variable infiltration capacity (VIC) model	Assessing the impacts of interannual change of climatic factors and land cover change on the change trend of interannual streamflow during 1959-2009.
Xie et al. (2015)	Three-North region of China	Variable infiltration capacity (VIC) model	Assessing the impacts of interannual change of climatic factors and multi-year average change of vegetation on the change trend of interannual streamflow during 1989-2009.
Wang et al. (2017)	China	Snowmelt-based water balance model (SWBM)	Exploring the runoff sensitivity to climate change for hydro-climatically different catchments in China during 1956-2016
Yang et al. (2019)	Loess Plateau of China	Variable infiltration capacity (VIC) model	Estimating the impacts of interannual change of climatic factors and multi-year average change of vegetation on the multi-year average change of streamflow between 1984-1999 and 2000-2015.
Wang et al. (2021)	The middle reaches of the Yellow River	Budyko-based elastic coefficient method	Assessing the impacts of multi-year average change of climatic factors and underlying surface condition on the multi-year average change of streamflow between 1956-1996 and 1997-2016
Zhai et al. (2021)	China	Variable infiltration capacity (VIC) model	Assessing the impacts of interannual change of climatic factors and multi-year average change of vegetation on the multi-year average change of streamflow between 1982-1984 and 1982-2016.
This study	Yellow River Basin	Variable infiltration capacity (VIC) model	Assessing the impacts of **interannual change and intra-annual temporal pattern change** of climatic factors and vegetation, and the **interactive effect** of climatic factors and vegetation change on the change trend of interannual streamflow during 1982-2018.

2 Study area and data

2.1 Study area

In the YRB, the area above the Tangnaihai (TNH) hydrologic station (100°09'E, 35°30'N) is defined as the headwater region. The Toudaoguai (TDG) station (111°04'E, 40°27'N) is the demarcation point between upper and middle reaches. The region between the TDG and Huayuankou (HYK) gauge (113°39'E, 34°55'N) is the middle reaches where the region between the TDG and Longmen (LM) gauge (110°35'E, 35°40'N) is the main sedimentation formation area of the YRB. The study area is the catchment above the Huayuankou station with a drainage area of 730,036 km^2 (~97% of the total area of the YRB), and the mean annual runoff in the study area accounts for ~98 % of that in the whole YRB (Tang et al., 2013). Areas of contribution for TNH, TDG, LM, and HYK are approximately 121,972 km^2, 367,898 km^2, 497,552 km^2, and 730,036 km^2, respectively. The study area is divided into 4 sub-regions (Source region, TNH-TDG, TDG-LM, LM-HYK) between the target gauge and the adjacent upstream gauge from TNH gauge to HYK gauge, as illustrated in the Figure 1.

110
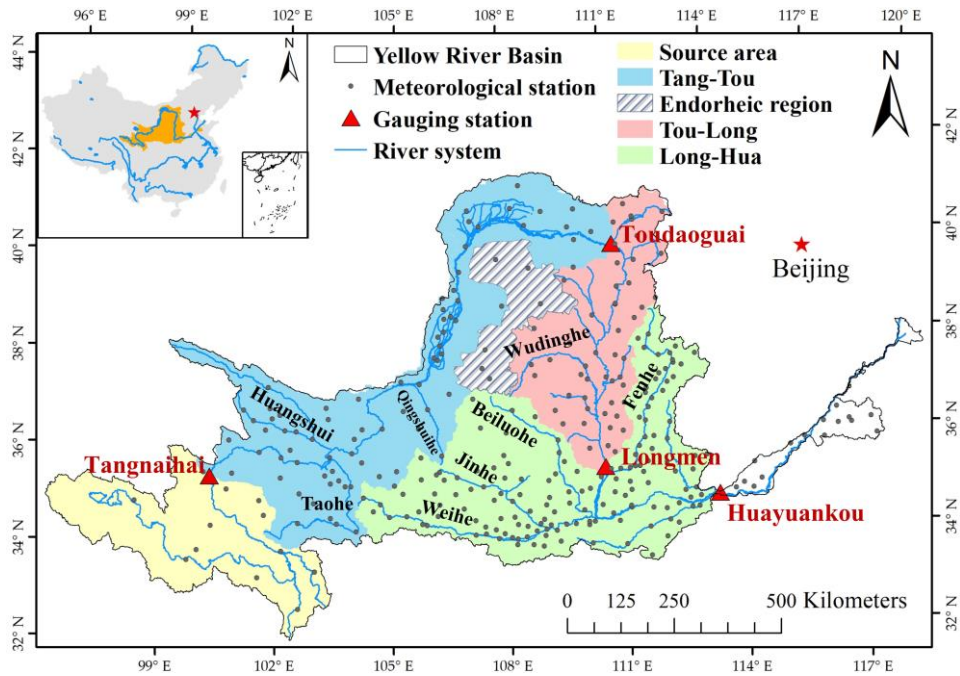
Figure 1. Spatial distribution of the meteorological and streamflow gauge stations in the YRB. The insert map shows location of the YRB in China.

2.2 Data sources

The observed daily data from 265 meteorological stations, including daily time series of precipitation, maximum temperature,
115 minimum temperature, and wind speed from 1980 to 2018 were obtained from the China Meteorological Administration
(http://data.cma.cn/). We calculated the daily mean temperature by averaging daily maximum and minimum temperature.
The 8-days time series of vegetation leaf area index (LAI) at 500 m from 1982 to 2018 used in this study was obtained from
The Global Land Surface Satellite (GLASS) product (Xiao et al., 2014) (http://glass-product.bnu.edu.cn/). We obtained land
cover data for every 5 years during 1985-2020 from the GLC_FCS30 product (Zhang et al., 2021), which was the first global
120 land cover product with fine classification system at 30 m (http://www.geodata.cn/). Elevation data obtained from the Shuttle
Radar Topography Mission (SRTM) digital elevation dataset at 90 m (https://www.gscloud.cn/) was used to delineate river
networks that are necessary for runoff routing of hydrological model. The soil texture data were derived from the 1-km
China soil map based harmonized world soil database (HWSD) (v1.1) (http://data.tpdc.ac.cn/en/). The China terrace
proportion map at 1 km resolution (Cao et al., 2021) in 2018 was download from https://doi.org/10.5281/zenodo.3895585.
125 Global surface water product at 30 m from 1984 to 2020 was available from the Joint Research Centre (JRC) (https://global-surface-water.appspot.com/download).

For runoff, there are 4 mainstream gauges shown in Figure 1. Monthly naturalized runoff from 1980 to 2018 were
provided by Yellow River Conservancy Commission of Ministry of Water Resources. Naturalized runoff at the target gauge
was estimated by adding ~~hman~~ human water use data from irrigation, industrial and domestic sectors over the drainage area

130 of the target gauge back to the observed runoff at the target gauge (Yuan et al., 2017; Zhang et al., 2020). We used naturalized runoff to calibrate hydrological model for simulating natural hydrological processes.

3 Methodology

3.1 Change detection of streamflow and influencing factors

We used the slope of the simple linear regression (Wang et al., 2022) to characterize the interannual change trend of
135 streamflow and influencing factors including precipitation, temperature, wind speed and LAI over the YRB. The t-test was used to examine the significance level of this trend. In addition, contribution of monthly streamflow change at a given month to the annual streamflow change was also determined by dividing the trend of monthly streamflow by the trend of annual streamflow.

Due to the changes of intra-annual temporal pattern in the precipitation and LAI are also able to affect the annual
140 streamflow, we taken the ratio of observed monthly to annual precipitation or LAI as the indicator of intra-annual temporal pattern in this study, and its change trend of each month was also analyzed. To explore more details on the relationship between temporal variability of precipitation and streamflow, double mass curve (Zhang et al., 2011) was performed to detect the abrupt change point and baseline period in the annual streamflow time series (Mu et al., 2007; Gao et al., 2010).

3.2 VIC model setup considering temporally explicit vegetation change

145 The VIC model uses the variable infiltration curve (Liang et al., 1994) to account for the spatial heterogeneity of runoff generation. It assumes that surface runoff for the upper two soil layers is generated by those areas where precipitation exceeds the storage capacity of the soil. The methods from the ARNO model (Todini, 1996) were used to describe base flow generation which only happened in the third soil layer. A separate routing model was then coupled with the VIC model to simulate streamflow (Lohmann et al. 1998), where the runoff generated in each grid cell is routed to selected points through
150 the channel network.

To balance the high cost of computation and the characterization of heterogeneous underlying surface, we performed simulations using the VIC model on a 0.1°×0.1° grid scale at a daily timestep. The inputs of the VIC model include meteorological forcings, vegetation parameters, land cover and soil parameters. The meteorological forcings were derived by interpolating gauged daily precipitation, maximum and minimum temperature, and wind speed from stations into a
155 resolution of 90 m based on the AUSPLINE software and DEM data, and we then calculated the spatial average of interpolated data within a grid cell, as illustrated in the Figure 2. By default setting of VIC model, ~~VIC simulation~~it only considers the climatology of vegetation (e.g., 12-month LAI), ~~and~~ and the ~~interannual change of~~ monthly LAI and land cover are stationary~~time invariant~~ in each year during the ~~implementation of the VIC model~~simulation period. Therefore, ~~Therefore, t~~the impacts of continuous interannual change of LAI and land cover types on hydrological processes rarely be

160   discussed in previous studies using VIC model (Xie et al., 2015; Yang et al., 2019; Zhai et al., 2021). In this study, the ~~VIC model~~ simulation scheme of VIC model (version 4.1.2.a) considering time-variant LAI was designed as the following two steps:

Step I: GLC_FCS30 product was firstly resampled to the same resolution (500 m) of LAI product. Owing to lack of yearly land cover data, the land cover data in the ith year from GLC_FCS30 product was used to represent the land cover from (i-

165   4)th year to ith year. We smoothed the 8-days LAI time series with the adaptive Savitzky–Golay filter (Chen, et al. 2004) to eliminate the abnormal LAI contaminated by cloud, signal errors from sensor, etc. The smoothed 8-days LAI was then aggregated to a monthly value with temporal averaging for each year. Finally, the area fractions and average monthly LAI value for each land cover type in each $0.1° \times 0.1°$ grid cell in each year were calculated respectively (Figure 2).

Step II: In the process of running VIC model, area fraction and monthly LAI for each land cover type in each grid cell in the

170   ith year were inputted into the VIC model, meanwhile the hydrological state at the last day in this year was saved. When starting hydrological simulation in the (i+1)th year, the area fraction and monthly LAI for each land cover type in each grid cell in the (i+1)th year and the hydrological state at the last day in the ith year were taken as the input data of VIC model. This cycle running scheme demonstrated in the Figure 2 can enable VIC model to successfully simulate hydrological process considering temporally explicit LAI and land cover change.

175   The soil physical parameters (e.g., field capacity, wilting point, and saturated hydraulic conductivity) are specified based on the soil texture of HWSD and the algorithms introduced by Maurer et al. (2002). The soil parameters that were not available from the HWSD were extracted from global soil datasets (Nijssen et al., 2001a). These soil data for VIC show great advantages for retrieving global soil moisture (Nijssen et al., 2001b) and river discharges (Nijssen et al., 2001a). The remaining numerical soil parameters were determined via model calibration following the method described in the section

180   3.3.
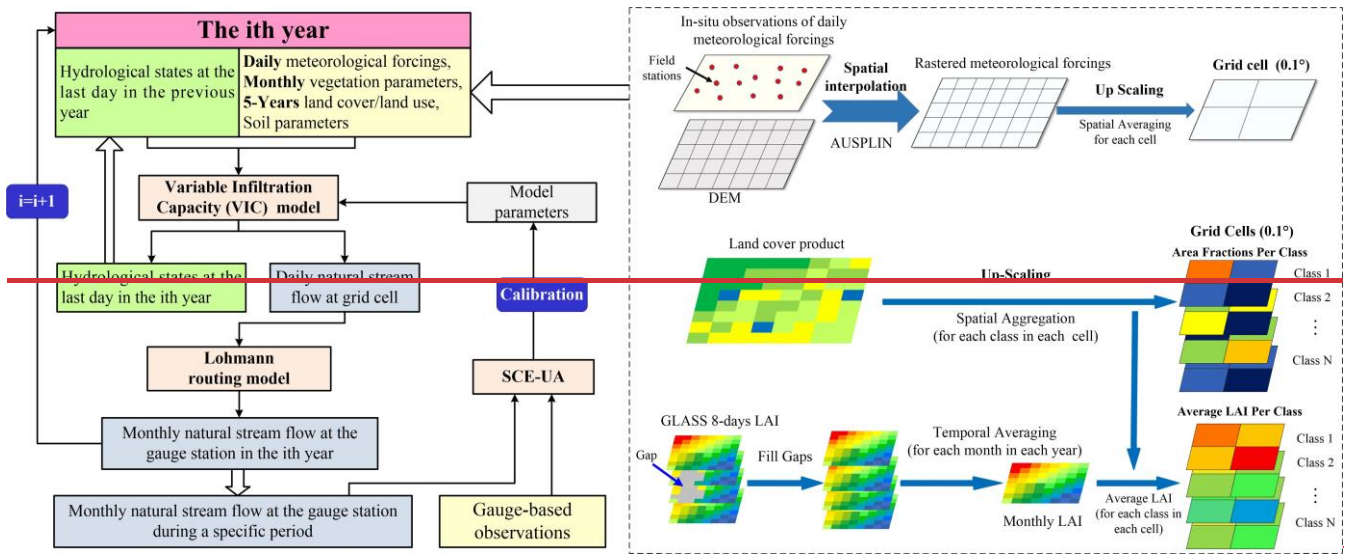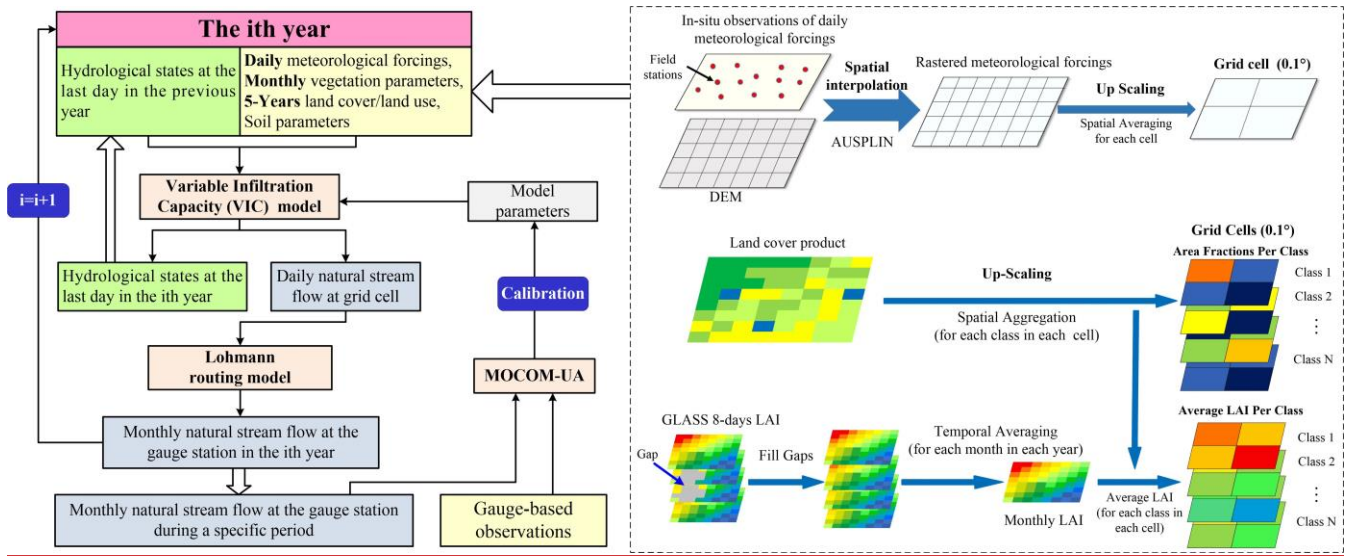
Figure 2. The flowchart of VIC model setup considering temporally explicit vegetation change

3.3 Model calibration and evaluation

The objective of this study was to investigate the contributions of changes in climate and vegetation to runoff changes, rather than to simulate runoff accurately from 1982 to 2018. Therefore, we adopted the baseline period to calibrate the 7 numerical soil parameters, including the infiltration parameter b, the depths of three soil layers (d_1, d_2 and d_3), and the three parameters in the base flow scheme (D_m, D_s, and W_s) (Xie et al. 2007; Shi et al. 2008), in different sub-regions.

To find the optimal parameter set, an optimization algorithm of the multi-objective complex evolution of the University of Arizona (MOCOM-UA) from Yapo et al. (1998) was implemented, and Nash–Sutcliffe efficiency (NSE), ~~average~~ relative bias (Bias) and root mean square error (RMSE) were used as the objective function to assess the model performance, as illustrated in Eq.(1)-Eq.(3). The automatic calibration was carried out by running the VIC model thousands of times ~~over each 0.1 degree grid cell within the YRB~~ during calibration period (1980-1993), of which the first two years (1980–1981) used for warm up, and the period of 1994-1999 is the validation period.~~.~~

$$NSE = 1 - \frac{\sum_{i=1}^{N}(Q_{obs,i}-Q_{sim,i})^2}{\sum_{i=1}^{N}(Q_{obs,i}-\overline{Q_{obs}})} \tag{1}$$

$$Bias = \frac{\sum_{i=1}^{N}Q_{sim,i}-\sum_{i=1}^{N}Q_{obs,i}}{\sum_{i=1}^{N}Q_{obs,i}} \tag{2}$$

$$RMSE = \sqrt{\frac{1}{N}\sum_{i=1}^{N}(Q_{sim,i}-Q_{obs,i})^2} \tag{3}$$

where Q_{sim} and Q_{obs} are the simulated and observed monthly streamflow, respectively, $\overline{Q_{obs}}$ is the arithmetic mean of the observed monthly runoff, i is the ith month, and N is the total number of months in calibration period.

This study assumes that the same amount of relative bias of annual streamflow trend during the calibration period will be transformed to the ~~scenario simulation~~simulation period, and this relative bias was then deducted when calculating impacts of climate and vegetation on runoff (Luan et al., 2020). In this way, we can minimize the impact of hydrological simulation error in attributing annual streamflow change trend.

3.4 Attributing the impacts of vegetation change and climate variation on streamflow trend

3.4.1 Reconstruction of de-trended climate variables and vegetation data

In this study, control conditions of climatic variables and LAI are defined as de-trended values rather than multi-year mean values adopted in other researches, because the interannual variability of the original time series can be preserved. The linear trend of the variable at annual scale was removed according to the processing steps in the study of Xie et al. (2015), and a similar de-trended strategy was successfully used by Tang et al. (2008) and Bai et al. (2019) to examine the impacts of climate change and vegetation. Daily precipitation and monthly LAI time series required for VIC model were reconstructed using Eq.(4)-Eq.(5), as follows:

$$P_{daily} = \frac{P_{daily}}{P_{monthly}} \times \frac{P_{monthly}}{P_{annual}} \times P_{annual} \tag{4}$$

$$LAI_{monthly} = \frac{LAI_{monthly}}{LAI_{annual}} \times LAI_{annual} \tag{5}$$

Where, P_{daily} is the daily precipitation time series, $P_{monthly}$ and $LAI_{monthly}$ are the monthly precipitation and LAI time series, P_{annual} and LAI_{annual} are the annual precipitation and LAI time series.

We generated the P_{daily} time series where the trend of annual value was removed using de-trended P_{annual} and original $\frac{P_{daily}}{P_{monthly}}$ and $\frac{P_{monthly}}{P_{annual}}$, and generated the P_{daily} time series where the trends of both annual value and intra-annual temporal pattern were removed using de-trended P_{annual} and $\frac{P_{monthly}}{P_{annual}}$ and original $\frac{P_{daily}}{P_{monthly}}$. Likewise, de-trended monthly LAI time series can be derived using same method.

3.4.2 Scenario simulation experiments

To explore the relative contributions of temporally explicit vegetation change and climate variation on annual streamflow trend, we designed several scenario simulations (Table 2). We first simulated the interannual streamflow trend when interannual change of annual values and intra-annual temporal pattern are de-trended for all climatic variables and LAI, and the land cover is fixed at the year of 1982 (Scenario S1), thus representing the baseline scenario under the control condition of unchanged climatic variable, vegetation and land cover during 1982-2018.

Table 2. Scenario simulation experimental design to attribute the effects of climate change and vegetation change on the runoff trend.

Scenarios	Climate variables		LAI and land cover		Purposes
	Interannual change	Interannual change of intra-annual temporal pattern of ~~rainfall~~precipitation	Interannual change	Interannual change of intra-annual temporal pattern of LAI	
S1	De-trended	De-trended	De-trended and fixed	De-trended	Estimating the runoff without any climate change and vegetation change
S2	Observed	De-trended	De-trended and fixed	De-trended	Estimating the impact of interannual change of climate variables
S3	Observed	Observed	De-trended and fixed	De-trended	Estimating the impact of intra-annual temporal pattern change of climate variables
S4	De-trended	De-trended	Observed	De-trended	Estimating the impact of interannual change of vegetation
S5	De-trended	De-trended	Observed	Observed	Estimating the impact of intra-annual temporal pattern change of vegetation
S6	Observed	Observed	Observed	Observed	Estimating the interactive effect of climatic factors and vegetation change

To isolate the effect of climate variables on streamflow trend, we designed two scenarios. In Scenario S2, annual value of

230 ~~specific~~ climate variable (precipitation, temperature and wind speed) varied one by one according to observation records while other variables vary according to control conditions in the S1. In Scenario S3, annual values of all climate variables and intra-annual temporal pattern of monthly precipitation vary according to observation records while other variables vary according to control conditions in the S1. The impacts of climate variables were calculated as follows:

$$Q_{P C_{inter}} = f(\text{~~C~~} P_{inter}) - f(control)$$

235
$$(6)$$

$$Q_{T_{inter}} = f(T_{inter}, P_{inter}) - f(P_{inter}) \tag{7}$$

$$Q_{WS_{inter}} = f(WS_{inter}, T_{inter}, P_{inter}) - f(T_{inter}, P_{inter}) \tag{8}$$

$$Q_{P_{intra}} = f(WS_{inter}, T_{inter}, P_{inter}\text{~~C~~}_{inter}, P_{intra}) - f(WS_{inter}, T_{inter}, P_{inter}\text{~~C~~}_{inter})$$

$$(9)$$

240
$$Q_C = Q_{P_{inter}} + Q_{T_{inter}} + Q_{WS_{inter}} + Q_{P_{intra}} = f(WS_{inter}, T_{inter}, P_{inter}, P_{intra}) - f(control) \tag{10}$$

Where $Q_{P C_{inter}}$, $Q_{T_{inter}}$ and $Q_{WS_{inter}}$ are impacts of interannual change of precipitation, temperature and windspeed, respectively, and $Q_{P_{intra}}$ is ~~each climate variable and~~ impact of intra-annual temporal pattern of precipitation ~~on the annual streamflow trend~~. Q_C represents the total impacts of all climate variables. $f(control)$, ~~$f(C_{inter})$~~ and $f(P_{inter}, T_{inter}, WS_{inter}, P_{intra})$~~$f(C_{inter}, P_{intra})$~~ are the simulated streamflow trends in the S1 ~~1, S2~~ and S3~~, respectively,~~ and $f(P_{inter})$, $f(T_{inter}, P_{inter})$~~,~~ and $f(WS_{inter}, T_{inter}, P_{inter})$ are the simulated streamflow trends in the S2.

245

To isolate the effect of vegetation on streamflow trend, we designed two more scenarios. In Scenario S4, annual values of LAI and land cover vary according to remote sensing observation records while other variables vary according to control

conditions in the S1, and both annual values of LAI and land cover and intra-annual temporal pattern of monthly LAI vary according to observation records while all climatic variables are de-trended in Scenario S5. The impacts of vegetation were

250 calculated as follows:

$$Q_{LAI_{inter}} = f(LAI_{inter}) - f(control) \tag{9 11}$$

$$Q_{LAI_{intra}} = f(LAI_{inter}, LAI_{intra}) - f(LAI_{inter}) \tag{10 12}$$

$$Q_{LAI} = Q_{LAI_{inter}} + Q_{LAI_{intra}} = f(LAI_{inter}, LAI_{intra}) - f(control) \tag{11 13}$$

Where $Q_{LAI_{inter}}$ and $Q_{LAI_{intra}}$ are impacts of interannual change of annual values and intra-annual temporal pattern of

255 vegetation on the annual streamflow trend. Q_{LAI} represents the total impacts of vegetation. $f(LAI_{inter})$ and $f(LAI_{inter}, LAI_{intra})$ are the simulated streamflow trends in the S4 and S5, respectively.

To identify the interactive effect of climate variables and vegetation on streamflow trend, we additionally designed the Scenario S6 to simulated the actual trend of streamflow based on dynamic climate variables and vegetation from 1982 to 2018, thus representing the combined effects from both climate and vegetation. Due to interactive effects of predictor

260 variables on response variable can be interpreted as the second-order or higher-order terms in Multi-point Taylor expansion (Bai et al., 2019), the interactive effect of climate variables and vegetation can be derived as follows:

$$Q_{C \times LAI} = f(C, LAI) - f(control) - Q_C - Q_{LAI} \tag{12 14}$$

Where $Q_{C \times LAI}$ is the interactive effect of climatic factors and vegetation on the annual streamflow trend. $f(C, LAI)$ is the simulated streamflow trend in the S6.

265 The impact of residual factors (e.g. non-vegetation underlying surface) was calculated by the residual method, as illustrated in the Eq.(13). The relative impact rate of each influencing factor on the annual streamflow trend were calculated using the Eq. (14).

$$Q_{Resi.} = Q_{nat} - Q_C - Q_{LAI} - Q_{C \times LAI} \tag{13 15}$$

$$Contr. X_i = \frac{Q_{X_i}}{\sum_{i=1}^{n} |Q_{X_i}|} \times 100\% \tag{14 16}$$

270 Where Q_{nat} is the change trend of naturalized streamflow. $Q_{Resi.}$ is the impact of residual factors on the annual streamflow trend. Q_{X_i} and $Contr. X_i$ are the impact and relative impact rate of ith (i=1,2,…,8) influencing factor respectively. The positive $Contr. X_i$ represents the positive impact to the streamflow change, and vice versa.

4 Results

4.1 Annual natural streamflow trend over YRB
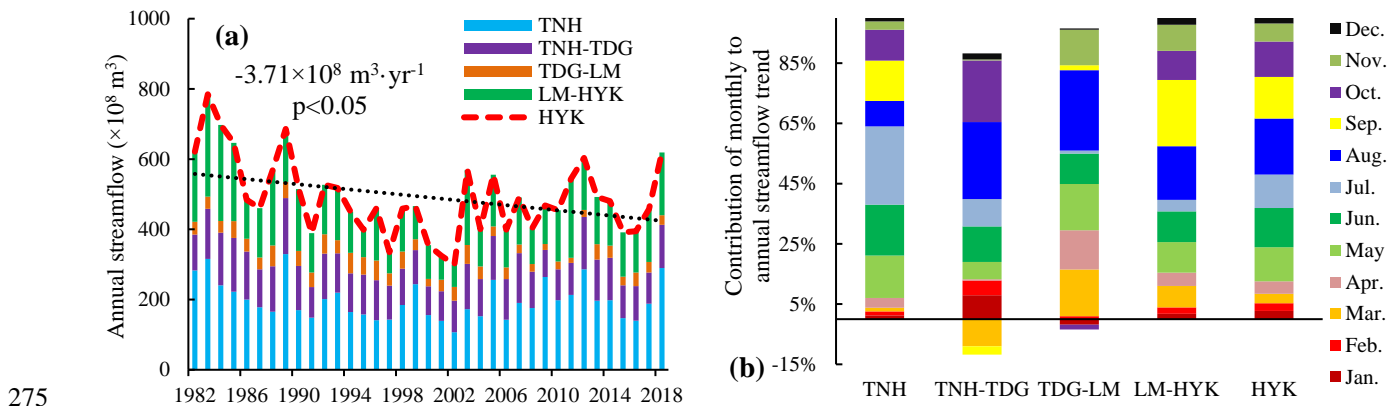
Figure 3. (a) Naturalized annual streamflows of HYK and different sub-regions, (b) contributions of monthly to annual streamflow trend of HYK and different sub-regions.

The Naturalized annual streamflows of HYK station, source region, TNH-TDG, TDG-LM and LM-HYK were provided in Figure 3(a). A significant decreasing trend was observed from the annual streamflow time series of HYK station during 1982-2018, with a negative trend of -3.71×10^8 m^3·yr^{-1}. Spatially, all sub-regions reported downward annual streamflow trends, with different contributions of 20.7%, 20.6%, 14.6% and 44% on the annual streamflow trend of HYK from source region to LM-HYK. Temporally, all monthly streamflow experienced negative trends at ~~HKY~~ HYK station, with a greatest reduction (18.6%) was found in August. Most monthly streamflow trends of four sub-regions were negative, and the greatest contributions of monthly trend to annual trend occurred in the July for source region, August for TNH-TDG and TDG-LM, and September for LM-HYK.

4.2 Temporally explicit change of climatic factors and vegetation

4.2.1 Interannual trend of climatic factors and LAI

The spatio-temporal change characteristics of interannual climate variables and LAI time series were investigated based on the linear slope analysis, as illustrated in the Figure 4, where interannual variability of region-averaged value and percentage of area with different significance level were summarized. The YRB experienced insignificantly positive trend in annual precipitation, with significant increases in only 4.6% of the basin, and areas with decreasing trend were mainly located at Huangshui basin and southeast in the LM-HYK. In the context of global warming, 97.5% of the YRB exhibited a significant increasing trend in annual mean temperature, with a change rate of 0.07°C·yr^{-1}. In contrast, significant decreasing trends in annual mean wind speed occurred over 78.2% of the YRB, while Taohe and Weihe basins had slight upward trends. For annual mean LAI, most of the YRB (72.5%) experienced a significant increasing trend, especially for the LM-HYK. The downward LAI trend occurred in ~~only~~ 15% of the~~ basin~~ study area, which was mainly distributed in the source region.

~~caused by the vegetation degradation in the source region and urbanization in the middle reaches.~~ A sharp increase of LAI trend in the TNH-TDG, TDG-LM and LM-HYK were noted after the year of 2000 associated with the implementation of Grain for Green Project (GFGP).
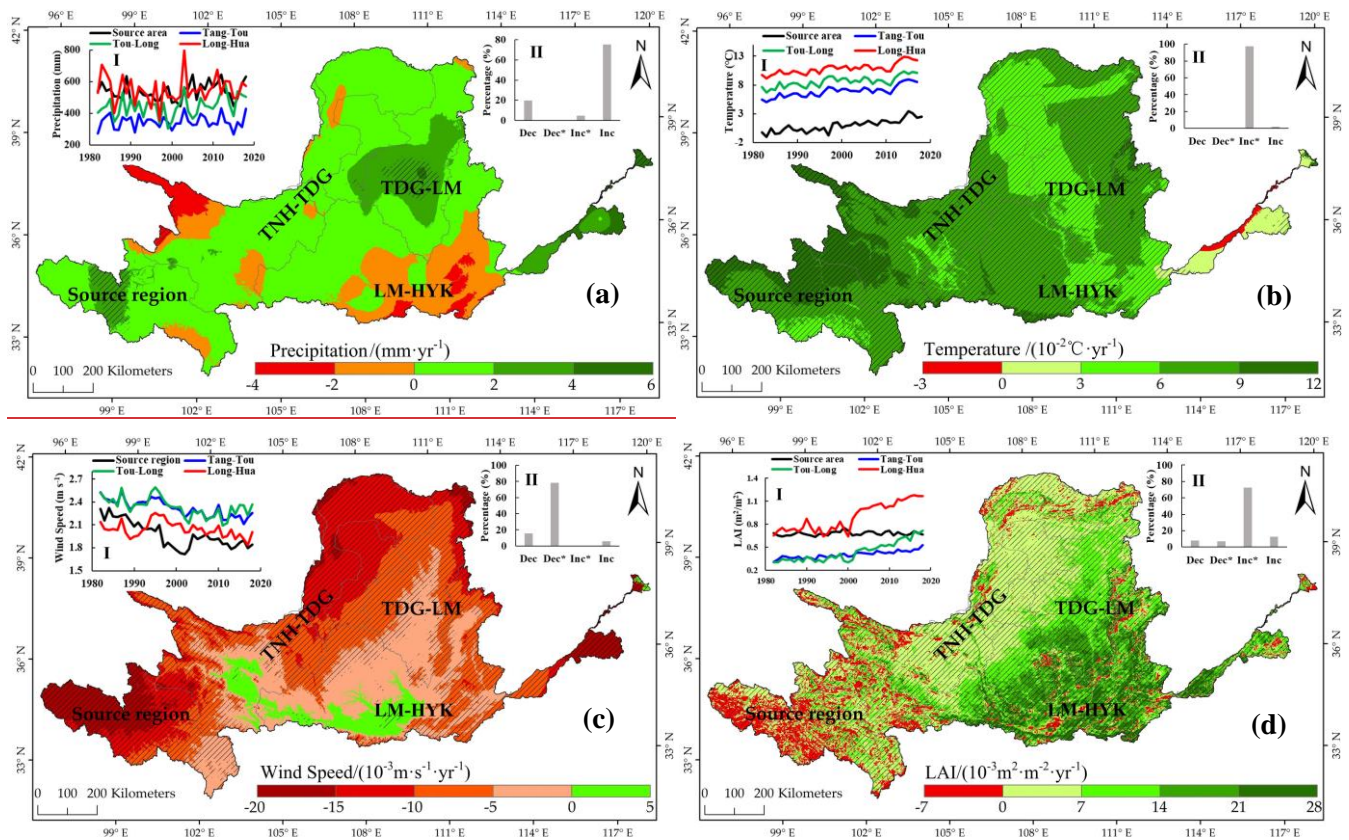
Figure 4. The spatio-temporal change of in precipitation (a), temperature (b), wind speed (c) and LAI (d). The insets (I) show the interannual variation of region-averaged variables. The insets (II) show the percentages (%) of the area with significant decrease (Dec*, p<0.05), insignificant decrease (Dec), insignificant increases (Inc), and significant increase (Inc*, p<0.05).

4.2.2 Interannual trend of intra-annual temporal pattern for precipitation and LAI

The statistics on the trends of monthly to annual precipitation ratio for four sub-regions were shown in the Figure 5. Negative trends primarily occurred between March and July, with July exhibiting the largest negative trends for all sub-regions except source region where a largest negative trend occurred in the June. Positive trends predominantly occurred between August and December, and September corresponded to the largest positive trends for all sub-regions except source region where a largest trend was observed in the August. It was indicated that the intra-annual temporal distribution of monthly precipitation has varied from 1982 to 2018, and positive contribution from the autumn season to annual precipitation has been progressively on the rise, whereas the contribution of summer has declined. ~~rainfall~~ Precipitation frequency caused by temporal pattern change of precipitation possibly influence the hydrological process over the YRB.

315
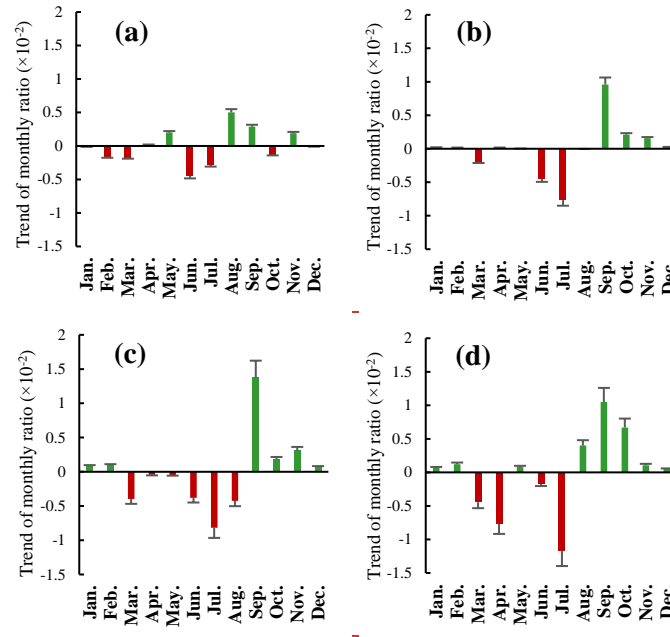
Figure 5. Trends in the ratio of the observed monthly to annual precipitation of subregions in (a) souce region, (b) TNH-TDG, (c) TDG-LM, (d) LM-HYK. The error bars represent the one standard deviation (s.d.).

The trends in the ratios of monthly to annual mean LAI for four sub-regions were shown in the Figure 6. Negative trends primarily occurred between June and September, whereas positive trends predominantly occurred remaining months. It was

320 obviously observed that the intra-annual temporal pattern of monthly LAI has also been varying during 1982-2018. Comparing with the upper reaches, the temporal pattern change was relatively great in the middle reaches, where positive contribution from the spring season to annual LAI has increased. Intra-annual change of evapotranspiration and soil moisture induced by temporal pattern change of LAI would influence the hydrological process over the YRB.
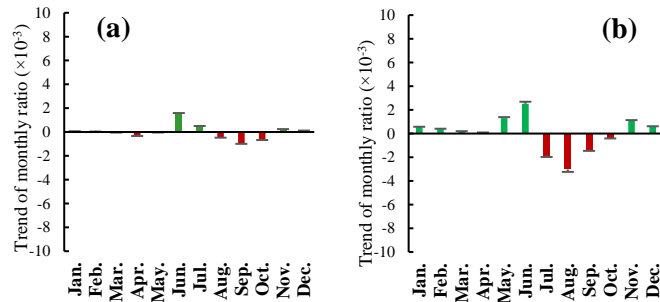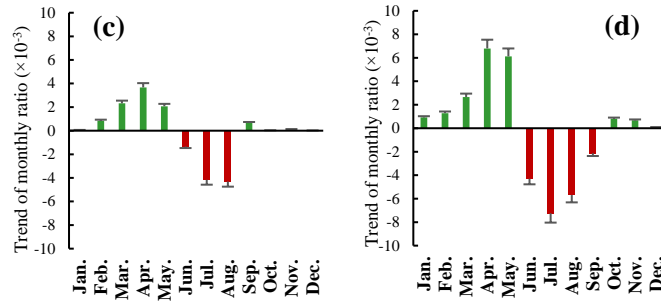
Figure 6. Trends in the ratio of the observed monthly to annual mean LAI of subregions in (a) souce region, (b) TNH-TDG, (c) TDG-LM, (d) LM-HYK. The error bars represent the 1 s.d.

4.3 Non-stationary relationship between precipitation and streamflow
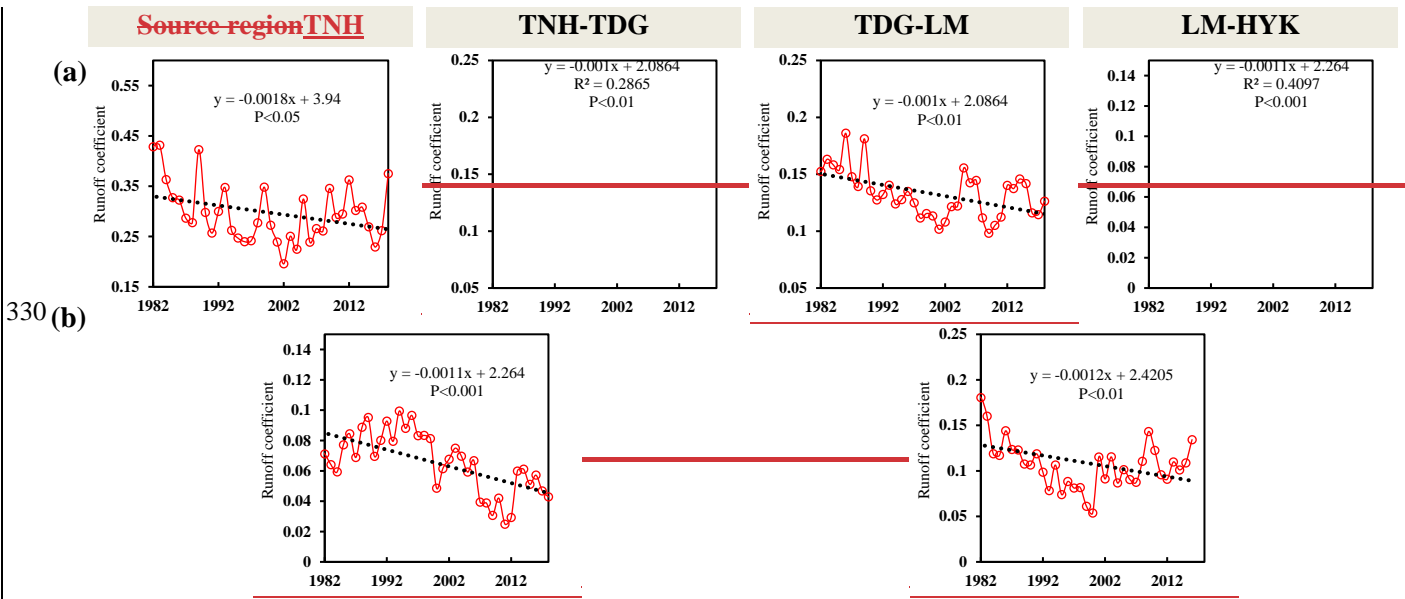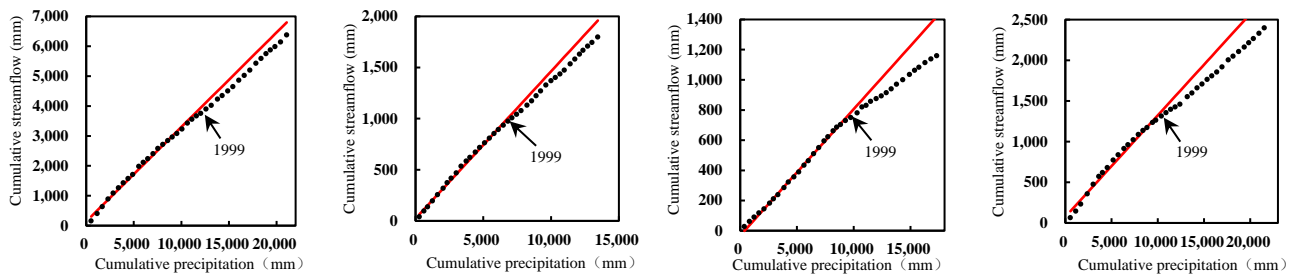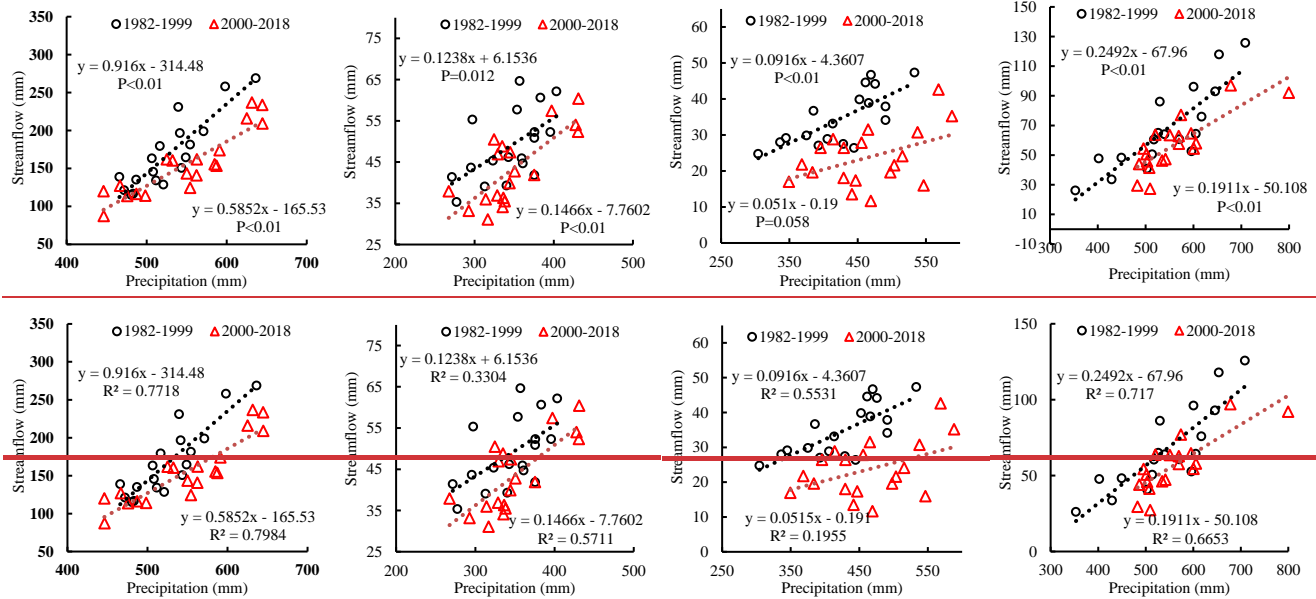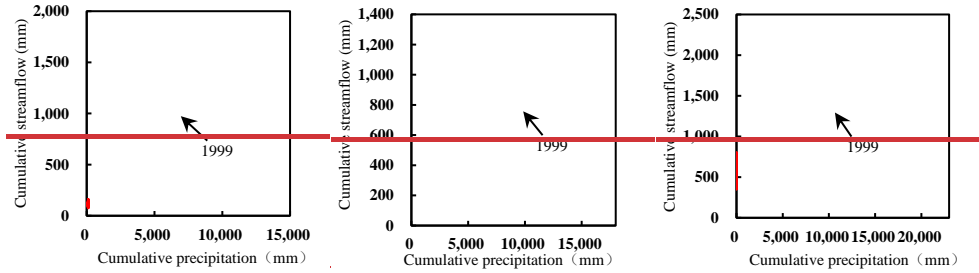
Figure 7. (a) The interannual change trend of annual runoff coefficiencts for ~~different~~4 sub-regions, (b) precipitation-streamflow double mass curves for 4 sub-regions, and (c) precipitation-streamflow relationships in the two periods of 1982-1999 and 2000-2018 for 4 sub-regions.

Runoff coefficients characterizing runoff yield capacity were calculated by streamflow divided by precipitation for all sub-regions, as illustrated in the Figure 7(a). It was found that overall trends in all sub-regions were negative during 1982-2018, although there were short-period upward trends from 2000 to 2018 in all sub-reigons excluding TDG-LM. To detect the abrupt change time of the realtionship between precipitation and streamflow, the cumulative curves of precipitation and streamflow of 4 sub-regions were calculated and plotted (Figure 7(b)). The discrepancy of cumulative precipitation and

streamflow observed from the Figure 7(b) indicated that the stationary precipitation-streamflow relationships have changed
in all sub-regions, and the deviation of the streamflow from precipitation is more significant in the middle reaches than upper
reaches. It is seen that significant abrupt changes in different sub-regions occurred in the same year of 1999. Thus, the study
period was divided into two periods: 1982-1999 and 2000-2018. It is clearly seen that from the Figure 7(c) the precipitation-
runoff relationship has significantly changed between these two periods, and the regression line of precipitation and runoff
during 1982-1999 always is above that during 2000-2018, which suggested that runoff in the period of 2000-2018 was
significantly reduced when same precipitation in the period of 1982-1999 occurred. Therefore, it is reasonable to split the
whole period into these two short-period. It could be concluded that the relationship between the annual precipitation and
streamflow presents a non-stationary state in the YRB from 1982 to 2018.

4.4 Model evaluation

According to the calculated abrupt change point from the precipitation-streamflow double mass curves in Figure 7, the
period of 1982-1999 was defined as the reference period, of which calibration and validation periods for calibrating VIC
parameters were 1982-1993 and 1994-1999 respectively. The seven model parameters calibrated in different drainage areas
are shown in the Table 3. The monthly hydrographs and average seasonal cycles of the simulated and naturalized
streamflows for different catchment regions are shown in the Figure 8, and the accuracy metrics of all simulations in the
Figure 8 are summarized in the Table 4respectively. According to the VIC simulations at HYK, the monthly NSE, RMSE
and Bias are 0.89, 387.4 mm and -1.6% for the calibration period and 0.8, 386.6 mm and 6.9% for the validation period
(Figure 8). Averaged across all four catchment regions, monthly NSE is 0.69, RMSE is 171.9 mm, and Bias is 5% during
calibration period, and monthly NSE is 0.6, RMSE is 156.8 mm, and Bias is 9.5% during validation period (Table 4Figure 8).
As per performance criteria given by Moriasi et al. (2007) (Table 3), simulation results indicate that the VIC model has a
good performance in simulating hydrological processes in not only subbasins and sub-regions. In addition, Figure 8Table 4
also shows the multi-year average monthly streamflow during 1982-1999, and NSE is larger than 0.85 in all catchment
regions, except for TDG-LM, thus indicating the seasonal cycles of streamflow also can be perfectly captured by VIC model
simulation.

-**Table 3.**

Calibrated parameters of VIC model for different drainage areas over YRB

Drainage areas	b	D_s	D_{smax}	W_s	b_1	b_2	b_3
TNH	0.374	0.514	23.559	0.671	0.091	0.100	1.021
TNH-TDG	0.313	0.454	18.686	0.771	0.102	0.172	0.497
TDG-LM	0.135	0.056	7.427	0.354	0.264	0.824	1.107
LM-HYK	0.151	0.123	18.973	0.530	0.134	0.465	0.812
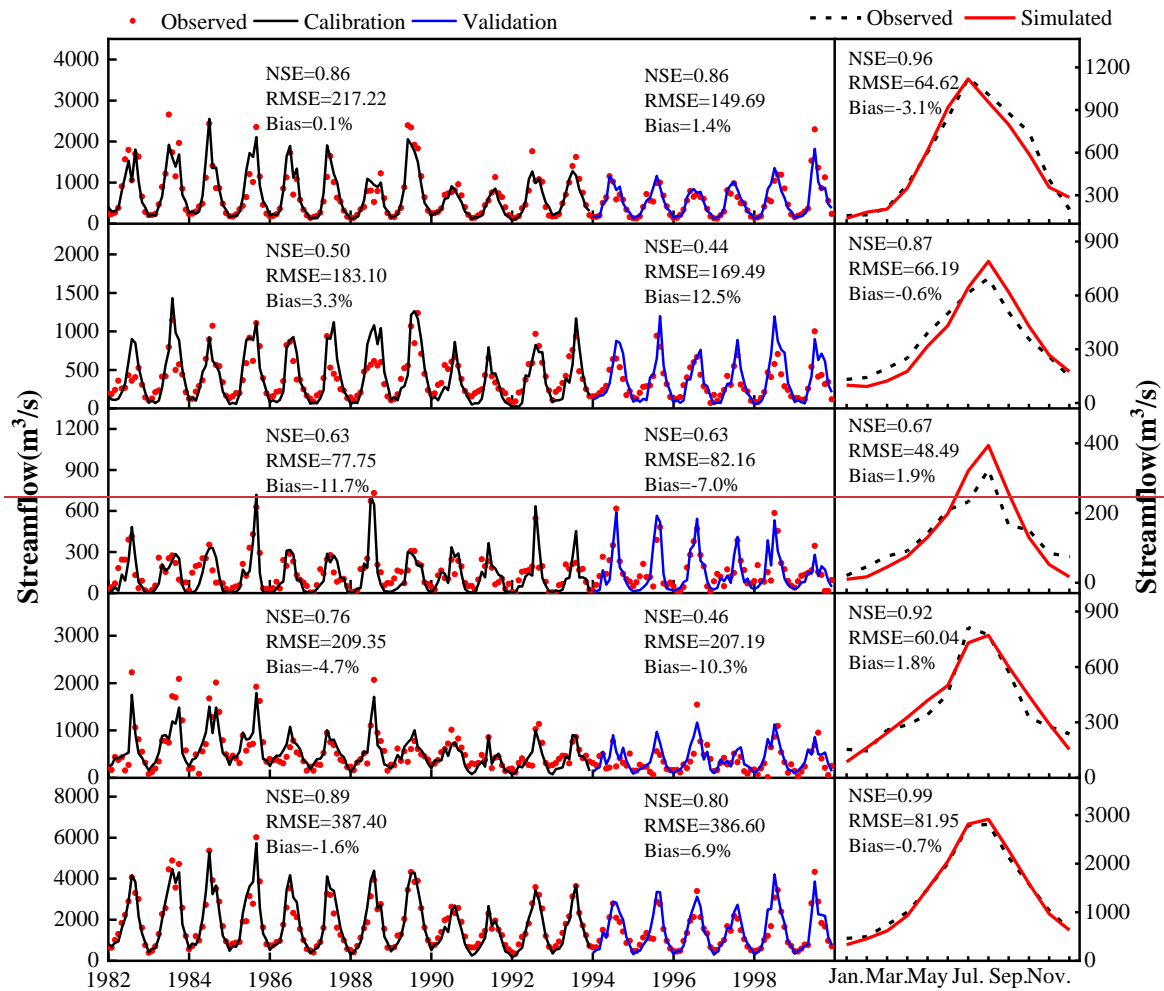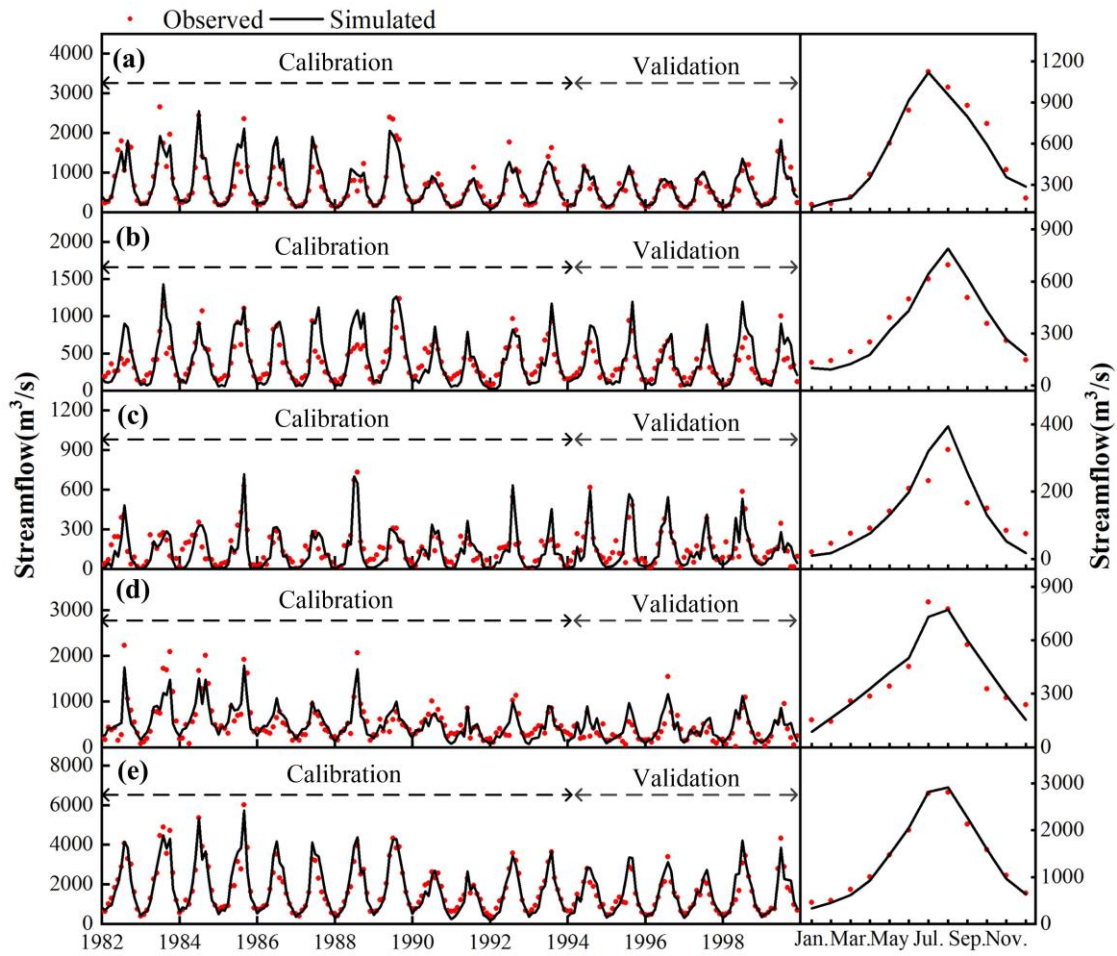
Figure 8. Comparisons of monthly streamflow and ~~seasonal cycles~~**seasonal cycles of streamflow** ~~of~~ **simulated by the** **VIC** ~~simulation~~ **and naturalized streamflow for different drainage areas during 1982-1999. (a) TNH, (b) TNH-TDG, (c) TDG-LM, (d) LM-HYK, (e) HYK**

Table 4 Model performance metrics of monthly streamflows and seasonal cycles of streamflows ~~and~~ ~~of o~~ **in different drainage areas**

Drainage areas	Monthly streamflow (1982-1999)						Multi-year average of seasonal cycles of streamflow (1982-1999)		
	Calibration period (1982-1993)			Validation period (1994-1999)					
	NSE	Bias	RMSE	NSE	Bias	RMSE	NSE	Bias	RMSE
TNH	0.86	0.1%	217.2	0.86	1.4%	149.7	0.96	-3.1%	64.6
TNH-TDG	0.5	3.3%	183.1	0.44	12.5%	169.5	0.87	-0.6%	66.2
TDG-LM	0.63	-11.7%	77.7	0.63	-7.0%	82.2	0.67	1.9%	48.5
LM-HYK	0.76	-4.7%	209.4	0.46	-10.3%	207.2	0.92	1.8%	60.0
HYK	0.89	-1.6%	387.4	0.8	6.9%	386.6	0.99	-0.7%	82.0

4.5 Impacts of influencing factors on the streamflow trend

The impacts and relative impact rates of eight influencing factors on the annual streamflow trends in different drainage areas were calculated using Eq.(6)-Eq.(14), as illustrated in the Figure 9 and Table 5. ~~For the HYK station, the contributions of all climate variables to the streamflow trend were positive excepting temperature, while larger negative effects from underlying surface change offset the slight positive effects of climate change on the streamflow trend (Figure 9).~~ From 1982 to 2018, the annual streamflow trend at HYK was -3.71×10⁸ m³·yr⁻¹, of which changes in interannual precipitation (P_inter), temperature (T_inter), wind speed (WS_inter), intra-annual temporal pattern of precipitation (P_intra), interannual LAI (LAI_inter), intra-annual temporal pattern of LAI (LAI_intra), interactive effects of climate variables and vegetation (Interactive), and residual underlying surface (Resi.) accounted for 15.1% (1.14×10⁸ m³·yr⁻¹), -23.5% (-1.77×10⁸ m³·yr⁻¹), 8.7% (0.66×10⁸ m³·yr⁻¹), 1.4% (0.1×10⁸ m³·yr⁻¹), -26.6% (-1.99×10⁸ m³·yr⁻¹) and -6% (-0.45×10⁸ m³·yr-1), -3.5% (-0.26×10⁸ m³·yr⁻¹), -15.2% (-1.14×10⁸ m³·yr⁻¹), respectively. For the HYK station, the contributions of all climate variables to the streamflow trend were positive excepting temperature, while larger negative effects from underlying surface change offset the slight positive effects of climate change on the streamflow trend (Figure 9). It is concluded that vegetation change was the dominant driving factor for the long-term decreasing trend of streamflow from 1982 to 2018 in YRB, meanwhile the effects in non-vegetation underlying surface changes (e.g. water and soil conservation engineering measures, permafrost melting, etc.) on reducing streamflow cannot be ignored.
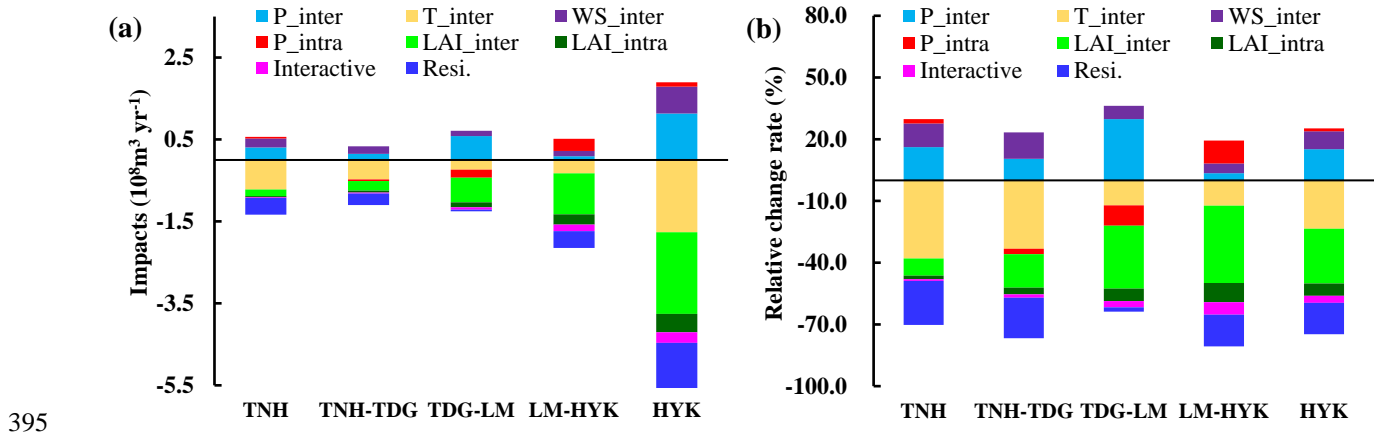
Figure 9. (a) Impacts and (b) relative impact rates of the different influencing factors on the annual streamflow trends in different drainage areas over YRB.

Table 5. Summary of the values of impacts and relative impacts rates of all influencing factors shown in the Figure 9

Influencing Factors	TNH Impact (10⁸m³·yr⁻¹)	TNH Rate (%)	TNH-TDG Impact (10⁸m³·yr⁻¹)	TNH-TDG Rate (%)	TDG-LM Impact (10⁸m³·yr⁻¹)	TDG-LM Rate (%)	LM-HYK Impact (10⁸m³·yr⁻¹)	LM-HYK Rate (%)	HYK Impact (10⁸m³·yr⁻¹)	HYK Rate (%)
P_inter	0.31	16.1%	0.15	10.5%	0.59	29.8%	0.09	3.5%	1.14	15.1%
T_inter	-0.72	-38.0%	-0.48	-33.2%	-0.24	-12.1%	-0.33	-12.3%	-1.77	-23.5%
WS_inter	0.22	11.5%	0.18	12.8%	0.13	6.5%	0.13	4.7%	0.66	8.7%
P_intra	0.04	2.1%	-0.04	-2.6%	-0.20	-9.9%	0.30	11.2%	0.10	1.4%

LAI_inter	-0.16	-8.3%	-0.23	-16.3%	-0.60	-30.5%	-1.00	-37.5%	-1.99	-26.6%
LAI_intra	-0.03	-1.7%	-0.05	-3.3%	-0.12	-6.1%	-0.25	-9.4%	-0.45	-6.0%
Interactive	-0.02	-0.8%	-0.02	-1.6%	-0.06	-3.1%	-0.16	-6.0%	-0.26	-3.5%
Resi.	-0.41	-21.4%	-0.28	-19.7%	-0.04	-2.1%	-0.41	-15.4%	-1.14	-15.2%

Due to divergent change of climate variables and underlying surfaces, the impact of different influencing factors on the streamflow trend in different sub-regions exhibited obvious spatial variability. Net total effect from interannual changes of all climate variables exhibited a negative influence on streamflow increase for all sub-regions, except for the TDG-LM with a positive impact of 0.47×10^8 m^3·yr^{-1}. The contribution of temperature on decreasing trend of streamflow in the upper reaches is greater than that in the middle reaches. Contributions of intra-annual temporal pattern change of precipitation on the streamflow trend illustrated obvious spatial heterogeneities. The impact of this factor was positive in the source region (2.1%) and LM-HYK (11.2%), whereas its negative effects were observed for the TNH-TDG (-2.6%) and TDG-LM (-9.9%). It was found that not only interannual increase of LAI, but also intra-annual LAI temporal pattern change had effects of reducing streamflow. Direct total impacts from vegetation change were negative for streamflow trend and accounted for -10% (-0.19×10^8 m^3·yr^{-1}), -19.5% (-0.28×10^8 m^3·yr^{-1}), -36.6% (-0.72×10^8 m^3·yr^{-1}), and -46.9% (-1.25×10^8 m^3·yr^{-1}) of the streamflow trends in source region, TNH-TDG, TDG-LM, and LM-HYK, respectively. Compared with direct effects of vegetation change, the two-way interactive effects of vegetation and climate variables were relatively low in all sub-regions. The impacts of residual underlying surface change were comparable to that of vegetation greening, with a maximum contribution of -21.4% (-0.41×10^8 m^3·yr^{-1}) occurred in the source region.

5 Discussion

5.1 Impacts of temporally explicit precipitation change on the precipitation intensity

Previous studies have suggested that precipitation is the main factor controlling runoff change with climate change (Dan et al., 2012; Wang et al., 2016; Liu et al., 2017). In this study, we further found that simulated annual streamflow trend could be changed by not only interannual precipitation (S2-S1) but also intra-annual monthly to annual precipitation ratio (S3-S2), which indicated that same annual precipitation with different intra-annual temporal pattern indeed affected the runoff generation process (Tang et al, 2008). Due to runoff yield in excess of infiltration is the dominant runoff mechanism where precipitationrainfall intensity is the crucial driving force over the most of YRB (Jin et al., 2020), we then focused on the impacts of interannual precipitation and intra-annual monthly to annual precipitation ratio on the precipitationrainfall intensity.

Different precipitation intensities, including light, moderate, heavy precipitation, are defined as daily precipitation amounts greater than 1, 10 and 25 mm, respectively in this region (Liu et al., 2018), and previous studies have proven that runoff was more sensitive to total amount of heavy precipitation (P$_{25}$) by analysing a large number of in-situ observation data (Liu et al., 2020). Therefore, the differences of interannual trends of P$_{25}$ between scenario S2 and S1 were calculated for each

meteorological station to indicate the impact of interannual precipitation on the heavy precipitation, as demonstrated in the Figure 10 (a). The meteorological stations with an increasing trend in P_{25} driven by interannual precipitation change accounted for 69.7%, with a maximum proportion of 80% in the TDG-LM, which caused the increase of annual streamflow (Figure 9).

Likewise, the impacts of intra-annual monthly to annual precipitation ratio on the P_{25} were analysed using the combination of scenario S3 and S2, as shown in the Figure 10 (b). The meteorological stations with an increasing trend in P_{25} driven only by intra-annual precipitation temporal patten change accounted for 58.9%, hence the overall effect of intra-annual temporal pattern change on the naturalized streamflow was positive during the study period. Spatially, increasing trends of P_{25} were observed in the majority of the stations within the source region (60%) and LM-HYK (68%), whereas the decreasing trend was dominant over the TNH-TDG and TDG-LM, which led to the spatial heterogeneity of the effects of intra-annual precipitation temporal patten change (Figure 9).
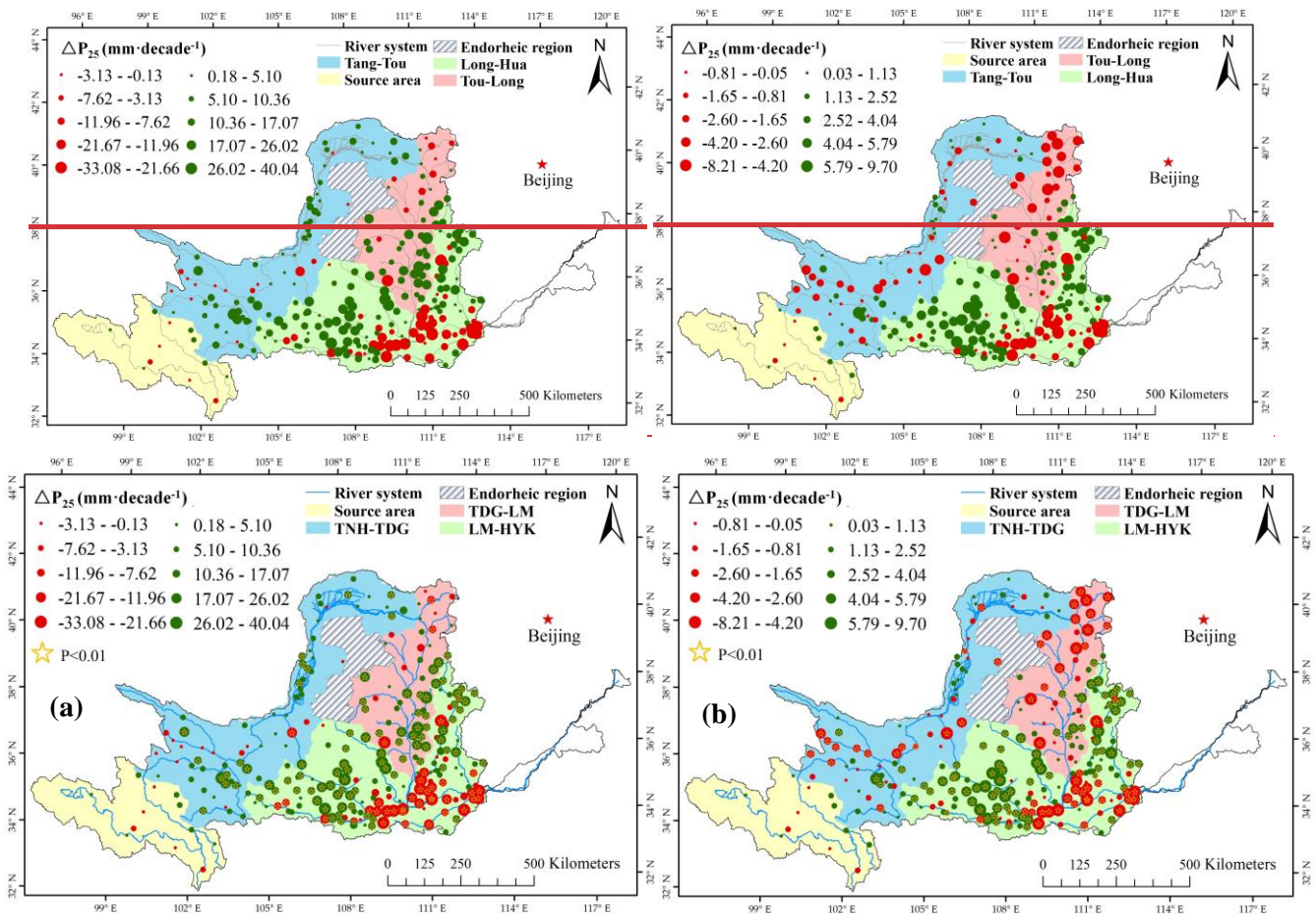
5.2 Potential driving mechanisms of temporally change of LAI
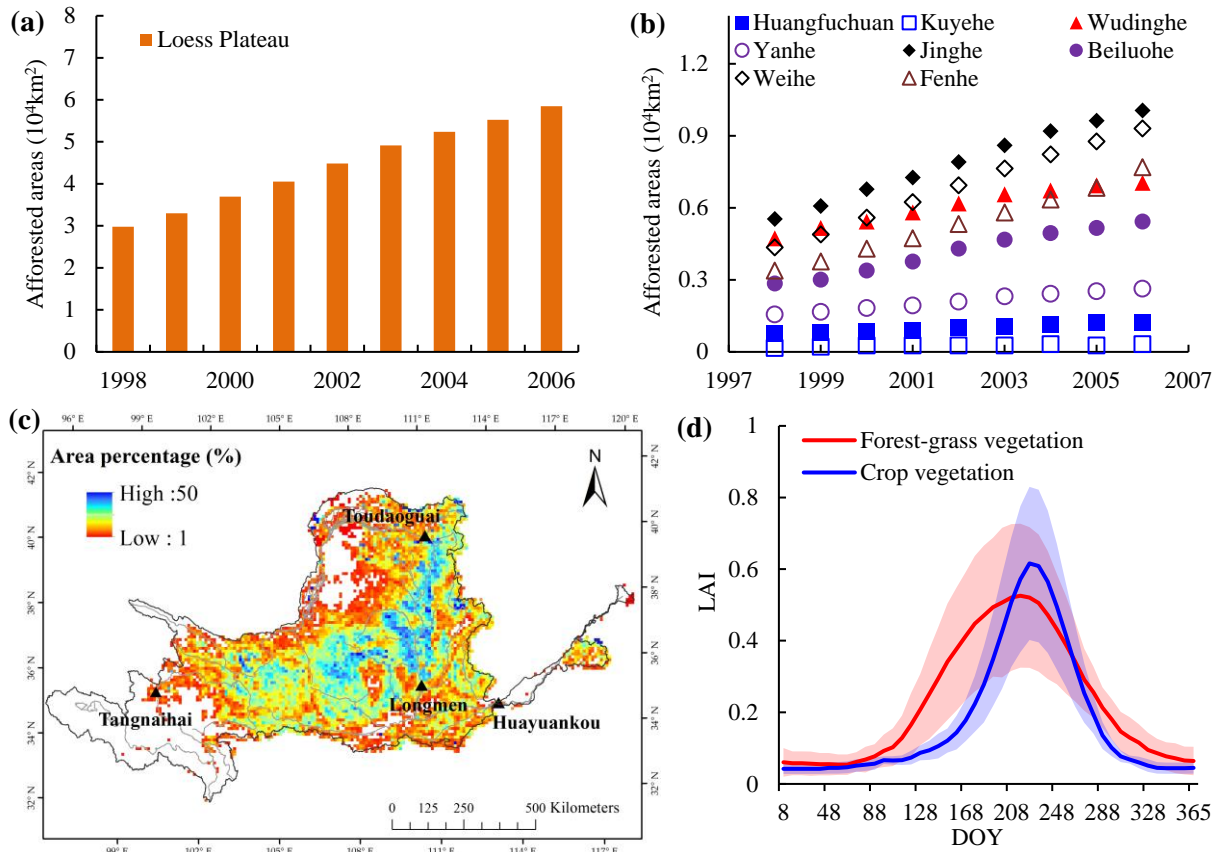
Figure 11. (a) Total afforested areas implemented in the Loess Plateau from 1998 to 2006; (b) Afforested areas in different watersheds between 1998 and 2006; (c) spatial distribution of area percentage of the conversion of cropland into forest-grass during 1985-2020 in each 0.1° grid cell; (d) The intra-annual variation of LAI at 8-days scale for typical forest-grass vegetation and crop vegetation, and the solid line and shaded area indicate the mean and ±1 s.d.

To mitigate increasingly devastating ecological environment and soil erosion problems, the Grain for Green Project (GTGP), which targets to convert farmland into forests and grasslands (Jia et al., 2014; Liu et al., 2014), have been implemented over the upper and middle reaches of the YRB since 1998. According to the statistical data from local forestry authorities (Yao et al., 2011), afforestation in the Loess Plateau has been mainly implemented during 1998-2006, and the afforested areas across the plateau increased greatly from 3×10^4 km² in 1998 to 5.9×10^4 km² in 2006 (Figure 11 (a)). Between 1998 and 2006, artificially planted trees and shrubs rapidly increased, and the afforested areas of the Fenhe, Weihe,

Beiluohe, Jinghe, Huangfuchuan, Yanhe, Kuyehe and Wudinghe watersheds increased by 128%, 113%, 93%, 82%, 76%, 66%, 55% and 49%, respectively, as shown in the Figure 11(b). Previous studies on the Loess Plateau have suggested that compared with climate change, the tree and grass planting activities was the dominant driving factor for the vegetation greening (Sun et al., 2015; Zhang et al., 2016; Bai et al, 2019). In addition, natural rehabilitation without intensive interference activities, such as grazing prohibition, may play an important role in vegetation restoration in the Loess Plateau (Cao et al., 2011).

To explore the vegetation type conversion caused by GTGP, area percentage of the conversion of cropland into forest-grass during study period for each 0.1° grid cell was calculated using the GLC_FCS30. Figure 11(c) shows that massive vegetation type conversion occurred in the TNH-HYK with a maximum percentage of 50%, which is partly proven by intense vegetation type conversion detected using Landsat time-series in the study of Wang et al. (2018). The Figure 11(d) depicts the phenological characteristics of typical crop vegetation and the forest-grass vegetation. The LAI of forest-grass vegetation in the spring and autumn season is obviously higher than that of farm crops, whereas LAI of crop vegetation in the summer season is slightly higher than that of forest-grass vegetation. Therefore, the massive vegetation type conversion from cropland into forest-grass vegetation could significantly alter the vegetation phenology~~phenological on the Loess Plateau~~, which could lead to the interannual trend of intra-annual monthly to annual LAI ratio increased in the spring and decreased in the summer (Figure 6). ~~Meanwhile, D~~due to phenology determines the start and end time of vegetation growth and is highly sensitive to climate change (Liang and Schwartz, 2009; Fu et al., 2019), climate warming has played an important role in advancing the spring phenology and delaying autumn phenology, and consequently extended the length of vegetation growing period across the globe (Piao et al., 2019; Menzel et al., 2020), especially for the semi-arid and semi-humid regions of China (Wu et al., 2015; Chen et al., 2022). In addition, the variations in micro-topography from slope land into flat terrace significantly increase soil moisture (Bai et al., 2019), which could also inevitably alter inter-annual change and intra-annual temporal pattern of LAI.

Recent studies have increasingly focused on the effect of vegetation phenology and growth on runoff. It is found that earlier spring phenology and delayed autumn phenology promote a longer growing season and can increase the period for plant transpiration, potentially resulting in larger transpiration and might reduce the river runoff (Piao et al., 2019; Geng et al., 2020; Wu et al., 2021; Chen et al., 2022). These results were consistent with the negative effect of intra-annual temporal pattern of LAI associated with phenology change on runoff simulated by VIC model considering explicit vegetation dynamics in this study.

5.3 Implication of considering temporally explicit vegetation change on hydrological effect assessment using VIC

In general, previous studies evaluated the hydrological effects of vegetation change using VIC model based on multi-year average LAI and vegetation types during different periods (Xie et al., 2015; Yang et al., 2019; Zhai et al, 2021) as a result of the model configurations of VIC (Liang et al., 1994; Xie et al., 2007). However, due to the smoothing effect of averaging,

490   multi-year average LAI is unable to fully capture the ~~spatiotemporal~~ vegetation continuous change, especially for the area with tremendous ecological restoration. Therefore, to explore the discrepancy in evaluating the hydrological effect of vegetation using VIC considering and without considering temporally explicit LAI change, we calculated the annual streamflow trend change by differencing simulation of scenario S1 and simulation with dynamic annual LAI observations while other variables varied under control conditions in the S1, and then calculated the streamflow trend change using the

495   combination of scenario S1 and simulation where annual LAI during 1982-1999 and 2000-2018 were fixed into the multi-year averages of corresponding periods respectively, while other variables varied same as S1. Likewise, the annual streamflow trend changes simulated by continuous and noncontinuous change of intra-annual temporal pattern of LAI were also calculated using same way.
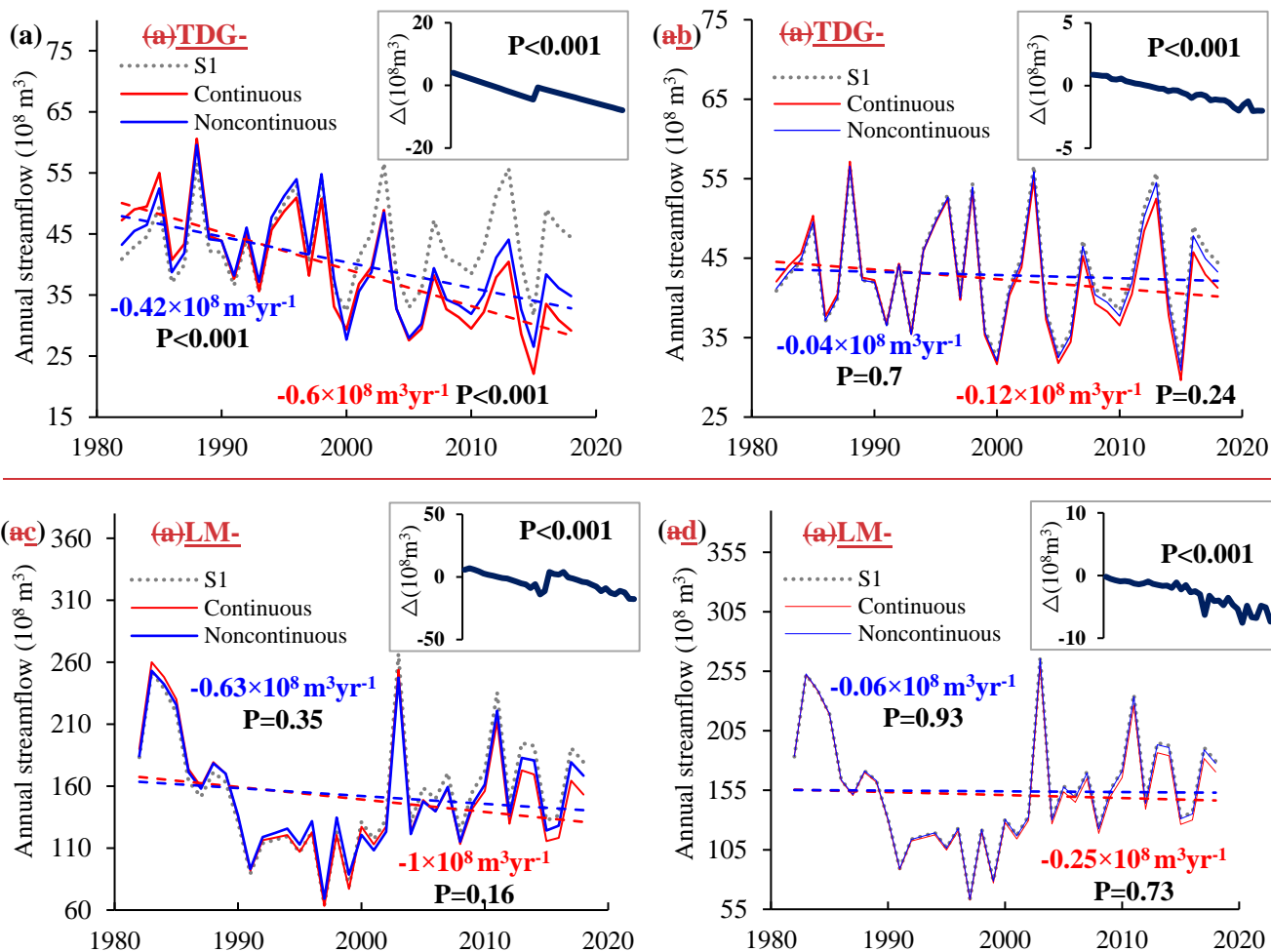
500
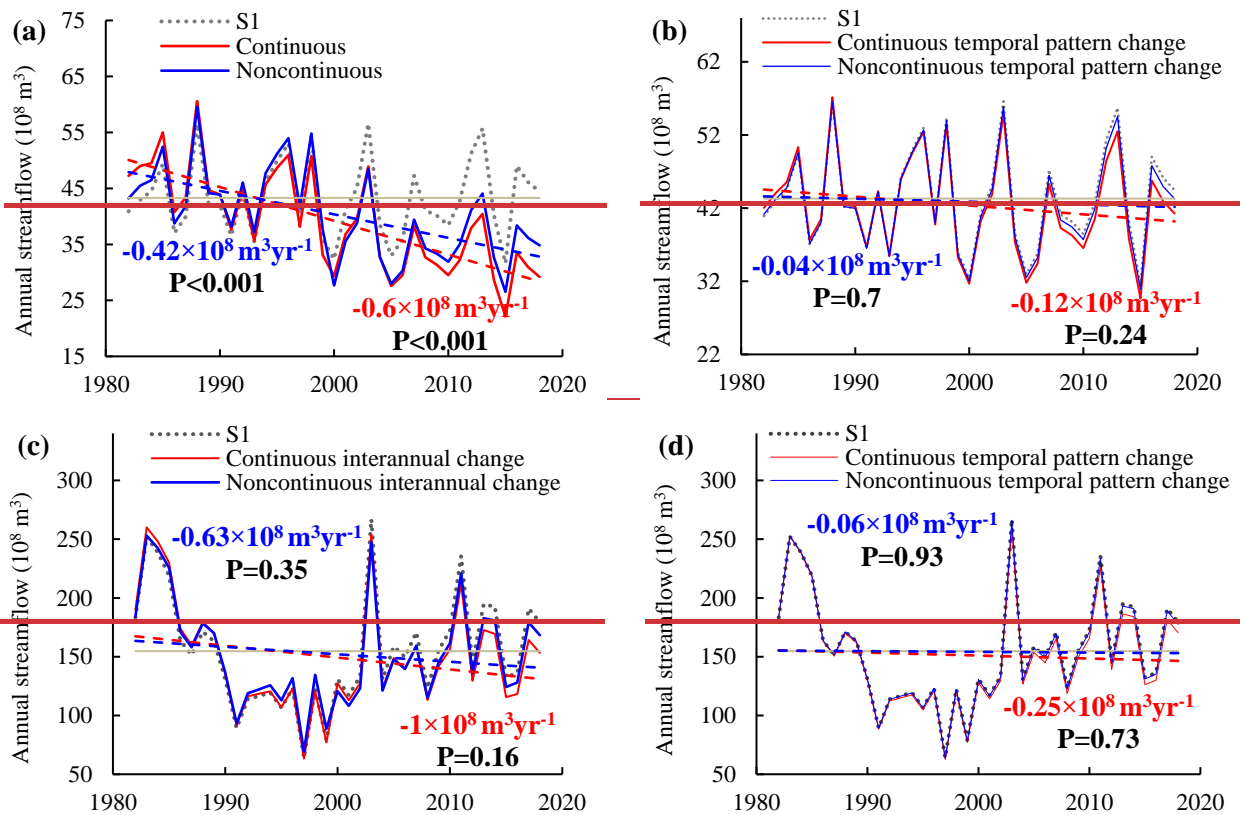
Figure 12. The comparison of simulated annual streamflow trend using VIC considering and without considering continuous dynamics of interannual LAI (a and c) and intra-annual temporal pattern of LAI (b and d) in the TDG-LM and LM-HYK. and intra-annual temporal pattern of LAI for the TDG-LM (a-b) and for the LM-TDG (c-d). The insets show the time-series of difference between simulated annual streamflow with VIC considering and without considering continuous LAI dynamics, and its significance level of change trend.

Figure 12 shows the comparison of simulated annual streamflow trend using VIC considering and without considering continuous dynamics of interannual LAI and intra-annual temporal pattern of LAI in the TDG-LM (Figure 12(a)~(b)) and LM-HYK (Figure 12(c)~(d)). It is found that compared with simulation with multi-year average LAIs change, the impact of vegetation simulated by continuous LAI change was increased by 42.9% and 58.7% for TDG-LM and LM-HYK respectively, and the impact of vegetation simulated by continuous intra-annual temporal pattern change was 3 times and 4.2 times of that simulated by noncontinuous inputs for TDG-LM and LM-HYK respectively. These results were consistent with the reported attribution of runoff change in the upland Mediterranean basin where reductions in runoff were less intense when afforestation was not considered in the hydrological model (Buendia et al., 2015). It should be noted that although the change trends of simulated annual streamflow (Figure 12(b)~(d)) are insignificant due to original interannual fluctuations were reserved in the scenario simulations, these trends become more significant when continuous LAI dynamics were

 considered in VIC simulation, and time-series of difference between simulated annual streamflow with VIC considering and without considering LAI dynamics show extremely significant change trend (P<0.001).
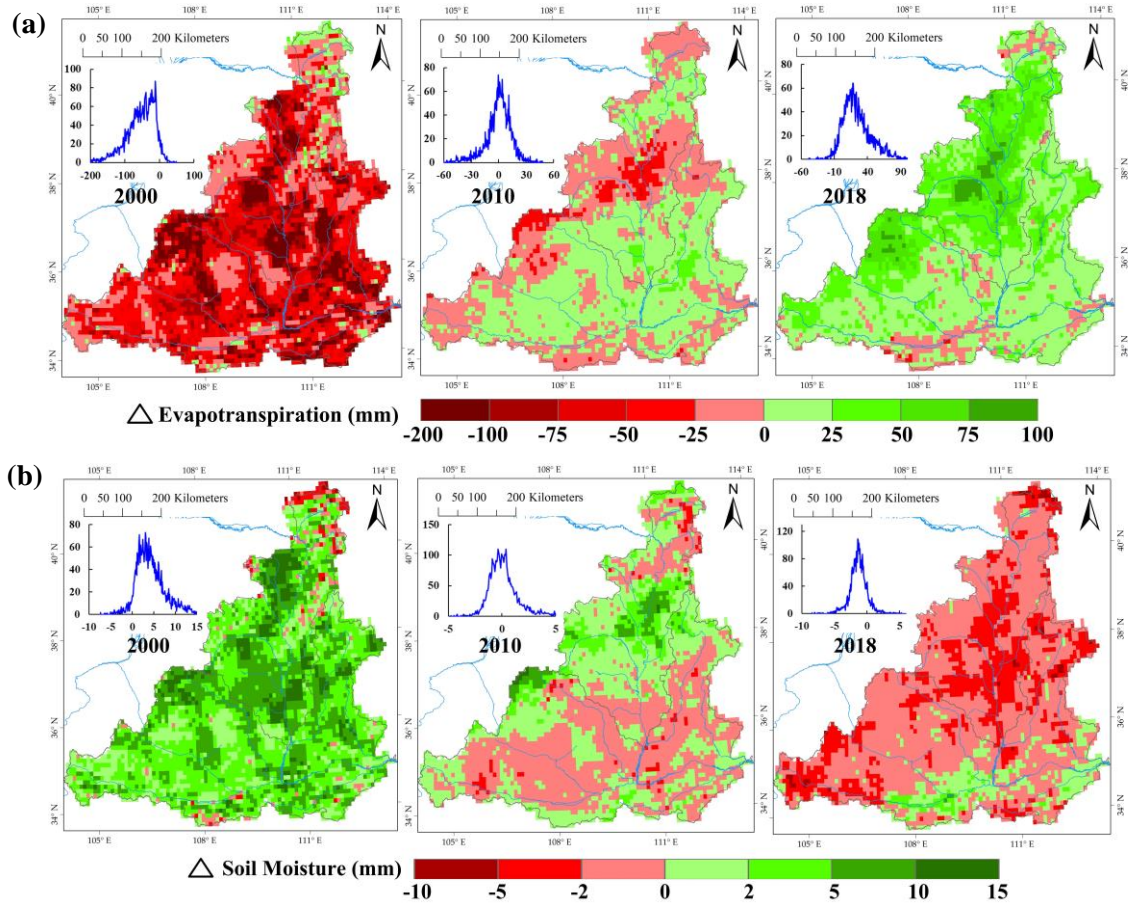
Figure 13. The difference between two simulations by VIC with dynamic LAI and fixed multi-year average LAI during 2000-2018 for annual total evapotranspiration (a) and annual average soil moisture (b) in the middle reaches in the year of 2000, 2010 and 2018. The insets show the statistical histogram of the difference value.

Previous studies focusing on this region at basin scale or regional scale have confirmed that massive vegetation greening has increased regional evapotranspiration through intense transpiration and canopy interception (Feng et al. 2016; Shao et al., 2019; Bai et al., 2019; Li et al., 2020), and caused a dried layer in the soil profile, interfering the vertical infiltration of soil water into the groundwater layer (Wang et al., 2011; Zhang et al., 2018), thus making negative impacts on the annual streamflow (Liang et al., 2015; Yang et al., 2019; Wang et al., 2021). Therefore, we further explore the impact of considering continuous LAI dynamic in VIC model on the simulations of total evapotranspiration and soil moisture of top-most layer in the middle reaches with significant vegetation increase. The discrepancies between VIC simulations with dynamic LAI and with fixed multi-year average LAI during 2000-2018 for annual total evapotranspiration and annual average soil moisture were calculated respectively, as illustrated in the Figure 13. The model using dynamic LAI tends to

predict lower (higher) evapotranspiration and higher (lower) soil moisture than the model using static multi-year average LAI in the year when LAI was lower (higher), and the discrepancies were especially large for maximum annual anomaly of LAI, which is consistent with the findings of previous studies in the North America (Vivoni et al., 2008; Tang et al., 2012; Liu et al, 2018). This could explain the less intense reduction in runoff when continuous LAI increase was not considered in

540   the hydrological simulation, as illustrated in the Figure 12~~.~~.

~~Recent studies have increasingly focused on the effect of vegetation phenology and growth on runoff. It is found that earlier spring phenology and delayed autumn phenology promote a longer growing season and can increase the period for plant transpiration, potentially resulting in larger transpiration and might reduce the river runoff (Piao et al., 2019; Geng et al., 2020; Wu et al., 2021; Chen et al., 2022). These results were consistent with the negative effect of intra-annual temporal~~

545   ~~pattern of LAI associated with phenology change on runoff simulated by VIC model considering explicit vegetation dynamics in this study.~~

5.4 Relationship between streamflow reduction and non-vegetation underlying surface change

To reduce sediment in the Yellow River, extensive water and soil conservation engineering measures including terraces and check dams were constructed over the Loess Plateau for mitigating soil erosion and intercepting sediment. According to

550   the terrace proportion map (Cao et al., 2021) and statistical data about terrace areas of eight main tributaries (Liu et al., 2021), built terrace was mainly distributed in the TNH-HYK (Figure 14(a)), and between 1979 and 2017 terrace areas of the Taohe, Huangshui, Qingshuihe, Beiluohe, Fenhe, Jinhe, Weihe subbasins and TDG-LM increased by 4.5, 4.9, 2.6, 3.0, 20.8, 10.4, 4.2 and 1.4 times respectively (Figure 14(b)), which indicated that change intensities of terrace areas in the TNH-TDG and LM-HYK were greater than that in the TDG-LM during the study period. Previous studies on the Loess Plateau have

555   confirmed that due to the slope land changes into flat land, terraces can damage the continuity of the slope and prolong the infiltration time, resulting in a poor hydrological connectivity and obvious runoff reduction (Tian et al., 2003; Bai et al., 2019). The study of Fu et al. (2020) also found that terrace plays critical role in reducing flood peak flow rate under extreme rainstorms.

In addition, check dams were increasingly built for blocking sediment from hillslope into river channel, and the

560   cumulative number of dams built above Tongguan station during 1982-2015 was 3700 and 3010 for large-sized and medium-sized dams respectively (Liu et al., 2020) (Figure 14(c)). Although check dam was originally designed to retain sediment, it still played significant role in storing water for local crop irrigation, which has been captured by the significant increase of surface water area derived from JRC product in the TNH-HYK, as shown in the Figure 14(d). It should be noted that greater change intensities in the terrace area and surface water area in the TNH-TDG and LM-HYK comparing with that

565   in the TDG-LM could probably explain the greater impact of residual factors on the streamflow reduction (Figure 9) in ~~the TNH-TDG and LM-HYK~~these two sub-regions, which is consistent with the spatial pattern of impacts of residual factors on the evapotranspiration increase for same sub-regions in the study of Wang et al. (2022).
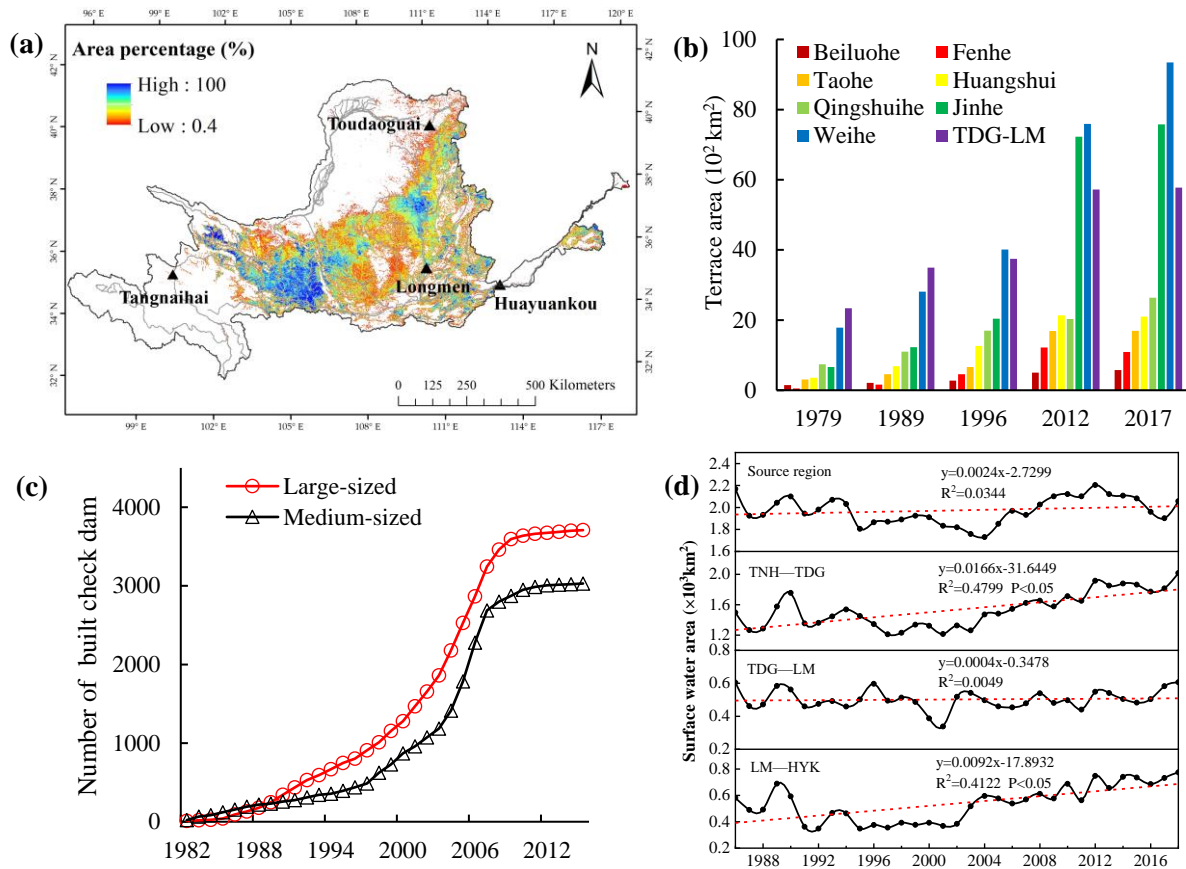
Figure 14. (a) Spatial distribution of area percentage of the terrace at 1km resolution in 2018; (b) Terrace areas in different main watersheds from 1979 to 2017; (c) Total number of check dams built above Tongguan station from 1982 to 2015; (d) Total areas of permanent water bodies in source region, TNH-TDG, TDG-LM and LM-HYK during 1986-2019.

For the source region where there are no significant changes in vegetation, terrace and check dam over last three decades, reported degradation of permafrost attributed to climate warming and human activities could enhance active layer thickness above permafrost and decrease duration of seasonally frozen ground (Wu and Zhang, 2008; Cheng and Jin, 2013). This would have profound effects on the hydrology by altering soil surface infiltration capacity and soil hydraulic conductivity (Jin et al., 2009, 2011). When permafrost is thawed, it can be changed from an aquitard to an aquifer in some areas and talik channels can be formed or enlarged, which facilitate surface water infiltration, river runoff decrease and groundwater recharge (Cheng and Jin, 2013). Cuo et al. (2013) have found it is highly possible that permafrost degradation has played a role in diminishing river runoff, meanwhile, increasing terrestrial water storage has also been confirmed in the study of Long et al. (2017).

5.5 Uncertainties

The gridded forcing data may introduce uncertainties in the simulations because these climate data are interpolated based on limited field observations. It would be better to merge high-accuracy microwave precipitation products and reanalysis data in the future. The GLASS LAI data were only used here, although differences exist between different LAI products, these LAI products generally consistent in the spatiotemporal changes across China (Piao et al., 2015; Zhu et al., 2016). Hence this would probably not change the general conclusions (Zhai et al, 2021).

~~The model parameters used in this study were calibrated using limited observations, and~~ It is difficult to accurately acquire naturalized streamflow due to some uncertainties of human water use data, especially from irrigation, which could explain the NSE lower than 0.5 in the validation period (Table 4) in the TNH-TDG and LM-HYK where there are large irrigated areas. In addition, all grid cells of sub-region were characterized with constant parameter dataset based on an idealized assumption. Hence further calibration should be conducted in more subbasins by collecting high-quality naturalized hydrological data and using hydrological model considering human water use to mitigate uncertainties of model parameters. ~~Hence further calibration and validation should be conducted in more subbasins by collecting more naturalized hydrological data to mitigate this potential uncertainty which may influence the model performance. However, the calibration and validation results showed that VIC simulations matched observations well in various periods in each sub regions (Figure 8), which ensures that the VIC model is applicable at regional scale in the YRB.~~

Scenario simulation method would ~~unavoidably~~ split the link and interaction between climate change and underlying surface change (Wu et al., 2017), which inevitably introduces a certain bias in quantifying the variation in streamflow induced by interannual and intra-annual changes of climate variables and vegetation. Even though the interactive effect was calculated by differencing the sum of variations in streamflow induced by climate and vegetation change and that induced by the coeffect in this study, this simplified method still cannot represent complicated feedback and response of climate and underlying surface change. ~~Due to the~~ LAI increase is always associated with land cover change ~~as a result of restoration projects~~, hence the vegetation's hydrological effect was considered as the total impact from LAI and land cover changes in this study. This inevitably involves the impacts of non-vegetated land cover conversion (e.g., urbanization), nevertheless this land cover change type only accounts for a very small proportion of YRB.

Due to the lack of water consumption data of coal mining and the effects of glaciers melting and permafrost degradation on the runoff generation were not considered during VIC simulation in this study, ~~,~~ the ~~effect~~ impacts ~~of~~ from coal mining, ~~glacier and~~ permafrost in analysing the relationship between non-vegetation underlying surface change and river runoff ~~was~~ were not ~~fully~~ further clarified~~considered~~. In addition, only one model was applied here, and water and soil conservation engineering measures were not considered in the model. The ~~analysis~~ conclusions of this study should be proven in further studies by combing the statistical model, lumped model, distributed model and machine learning model.

6 Conclusion

YRB hydrological regimes have exhibited changes over the past decades as manifested by decreases in annual streamflow. Here, daily meteorological, monthly LAI and yearly land use/cover time-series data were coupled in the VIC hydrological model to ~~disentangle~~ clarify the contributions from temporally explicit changes of climate variables and vegetation on the natural streamflow trend during 1982-2018. Comparing with the attribution of streamflow trend using the VIC simulation without considering dynamic LAI, simulations with dynamic LAI can better capture the temporally explicit variations of evapotranspiration and soil moisture induced by vegetation, which enables VIC to reflect the cumulative effects of vegetation changes on the streamflow. Results show that total effects from vegetation greening composed of interannual LAI increase and intra-annual LAI temporal pattern change, primarily induced by large-scale ecological restoration, might play a dominant role in the natural streamflow reduction of YRB over last decades. The impact from non-vegetation underlying surface change is also great due to the water storage capacities of terraces and check dams. Positive contribution from precipitation and wind speed almost offset the negative effect from temperature on the hydrological regimes. It should be noted that the intra-annual precipitation temporal pattern change is able to affect the streamflow trend by altering the precipitation intensity that is sensitive to the runoff in the YRB.

Code and data availability. VIC is open-source macroscale hydrological model (https://vic.readthedocs.io/en/master/). Meteorological data was obtained from the China Meteorological Administration (http://data.cma.cn/). Time-series LAI data was obtained from The Global Land Surface Satellite (GLASS) product (http://glass-product.bnu.edu.cn/). GLC_FCS30 product was downloaded from http://www.geodata.cn/. China soil map based harmonized world soil database (HWSD) (v1.1) was download from http://data.tpdc.ac.cn/en/. The China terrace proportion map was download from https://doi.org/10.5281/zenodo.3895585. Global surface water product was available from the Joint Research Centre (JRC) (https://global-surface-water.appspot.com/download).

Author contributions. The paper has been authored by ZW with contributions from all the co-authors. ZW, QT and DW contributed to the conceptualization and methodology. ZW ran the VIC model and performed the scenario simulations. PX provided naturalized streamflow data and analysed its temporal dynamics. RX provided the meteorological dataset and a high-performance computing platform to run VIC model. PX, RX, PS and FF contributed to the writing and revision of the manuscript.

Competing interests. The contact author has declared that neither they nor their co-authors have any competing interests.

Acknowledgements. We are grateful to Beijing Normal University for providing long-term GLASS products. We thank Dr. Zhang Xiao in the Aerospace Information Research Institute, Chinese Academy of Science for providing the land cover products of different years. We also thank Dr. Zhang Xuejun in China Institute of Water Resources and Hydropower Research for his assistance in the run and calibration of VIC model.

Financial support. This study was supported by the Joint Funds of the National Natural Science Foundation of China (U2243210), and National Natural Science Foundation of China (41730645), and Key Science and technology Project of Ministry of Water Resources (SKR-2022017).

Review statement.

References

1. Bai, J., Yang, S., Zhang, Y., Liu, X., and Guan, Y.: Assessing the Impact of Terraces and Vegetation on Runoff and Sediment Routing Using the Time-Area Method in the Chinese Loess Plateau, Water., 11(4), 803, http://doi.org/10.3390/w11040803, 2019.

2. Bai, M., Mo, X., Liu, S., and Hu, S.: Contributions of climate change and vegetation greening to evapotranspiration trend in a typical hilly-gully basin on the Loess Plateau: China, Sci. Total Environ., 657, 325-339, https://doi.org/10.1016/j.scitotenv.2018.11.360, 2018.

3. Bao, Z., Zhang, J., Wang, G., Chen, Q., Guan, T., Yan, X., Liu, G., Liu, J., and Wang, J.: The impact of climate variability and land use/cover change on the water balance in the Middle Yellow River Basin, China, J. Hydrol., 577: 123942, https://doi.org/10.1016/j.jhydrol.2019.123942, 2019.

4. Buendia, C., Bussi, G., Tuset, J., Vericat, D., Sabater, S., Palau, A., and Batalla, RJ.: Effects of afforestation on runoff and sediment load in an upland Mediterranean catchment, Sci. Total Environ., 540, 144-157, http://doi.org/10.1016/j.scitotenv.2015.07.005, 2015.

5. Cao, B., Yu, L., Naipal, V., Ciais, P., Li, W., Zhao, Y., Zhang, T., Chen, D., Liu, Z., and Gong, P.: A 30 m terrace mapping in China using Landsat 8 imagery and digital elevation model based on the Google Earth Engine, Earth Syst. Sci. Data, 13, 2437–2456, https://doi.org/10.5194/essd-13-2437-2021, 2021.

6. Cao, S., Chen, L., Shankman, D., Wang, C., Wang, X., and Zhang, H.: Excessive reliance on afforestation in China's arid and semi-arid regions: lessons in ecological restoration, Earth Sci. Rev., 104(4), 240-245, https://doi.org/10.1016/j.earscirev.2010.11.002, 2011.

680 7. Chang, J., Zhang, H., Wang, Y., and Zhu, Y.: Assessing the impact of climate variability and human activities on streamflow variation, Hydrol. Earth Syst. Sci., 20, 1547-1560, https://doi.org/10.5194/hessd-12-12747-2015, 2016.

8. Chen, J., Jönssonc, P., Tamura, M., Gu, Z., Matsushita, B., and Eklundh, L.: A simple method for reconstructing a high-quality NDVI time-series data set based on the Savitzky-Golay filter, Remote Sens. Environ., 91(3-4), 332-344, https://doi.org/10.1016/j.rse.2004.03.014, 2004.

685 9. Chen, S., Fu,Y., Geng, X., Hao Z., Tang, J., Zhang, X., Xu, Z., and Hao, F.: Influences of Shifted Vegetation Phenology on Runoff Across a Hydroclimatic Gradient, Front. Plant Sci., 12, 802664, https://doi.org/10.3389/fpls.2021.802664, 2022.

10. Cheng, G. and Jin, H.: Permafrost and groundwater on the Qinghai-Tibet Plateau and in northeast China. Hydrogeol. J., 21, 5-23, 175, http://doi.org/10.1007/s10040-012-0927-2, 2013.

690 11. Cuo, L., Zhang, Y., Gao, Y., Hao, Z., and Cairang, L.: The impacts of climate change and land cover/use transition on the hydrology in the upper Yellow River basin, China, J. Hydrol., 502, 37-52, https://doi.org/10.1016/j.jhydrol.2013.08.003, 2013.

12. Dan, L., Ji, J., Xie, Z., Chen, F., Wen, G., and Richey, J. E.: Hydrological projections of climate change scenarios over the 3H region of China: A VIC model assessment, J. Geophys. Res., 117, 148-227, https://doi.org/10.1029/2011JD017131, 2012.

695
13. Feng, X., Fu, B., Piao, S., Wang, S., Ciais, P., Zeng, Z., Lü, Y., Zeng, Y., Li, Y., Jiang, X., and Wu, B.: Revegetation in China's loess plateau is approaching sustainable water resource limits, Nat. Clim. Chang, 6, 1019-1022, https://doi.org/10.1038/nclimate3092, 2016.

14. Ford, T. W. and Quiring, S. M.: Influence of MODIS-derived dynamic vegetation on VIC-simulated soil moisture in Oklahoma, J. Hydrometeorology, *14*(6), 1910-1921. DOI:10.1175/JHM-D-13-037.1, 2013.

15. Fu, B.: 1981. On the calculation of the evaporation from land surface, Chinese J. Atmospheric Sci., 5(1), 23-31 (in Chinese).

16. Fu, G., Chen, S., Liu, C., and Shepard, D.: Hydro-climatic trends of the Yellow River basin for the last 50 years, Clim. Change, 65, 149-178, https://doi.org/10.1023/B:CLIM.0000037491.95395.bb, 2004.

705 17. Fu, S., Yang, Y., Liu, B., Liu, H., Liu, J., Liu, L., and Li, P.: Peak flow rate response to vegetation and terraces under extreme rainstorms, Agric. Ecosyst. Environ., 288, 106714, http://doi.org/10.1016/j.agee.2019.106714, 2020.

18. Fu, Y., Zhang, X., Piao, S., Hao, F., Geng, X., Vitasse, Y., and Janssens, I. A.: Daylength helps temperate deciduous trees to leaf-out at the optimal time, Glob. Chang Biol., 25(7), 2410-2418.https://doi.org/10.1111/gcb.14633, 2019.

19. Gao, P., Mu, X., Wang F., and Li, R.: Changes in streamflow and sediment discharge and the response to human activities in the middle reaches of the Yellow River, Hydrol. Earth Syst. Sci., 15(1):347-350. https://doi.org/10.5194/hess-15-1-2011, 2010.

20. Geng, X., Zhou, X., Yin, G., Hao, F., Zhang, X., Hao, Z., Fu, Y.: Extended growing season reduced river runoff in Luanhe River basin, J. Hydrol., 582, 124538, https://doi.org/10.1016/j.jhydrol.2019.124538, 2020.

21. Haddeland, I., Lettenmaier, D. P., and Skaugen, T.: Effects of irrigation on the water and energy balances of the Colorado and Mekong river basins, J. Hydrol., 324, 210-223, http://doi.org/10.1016/j.jhydrol.2005.09.028, 2006.

22. Hu, Y., Maskey, S., Uhlenbrook, S., and Zhao, H.: Streamflow trends and climate linkages in the source region of the Yellow River, China, Hydrol. Process, DOI:10.1002/hyp.8069, 2011.

23. Jia, X., Fu, B., Feng, X., Hou, G., Liu, Y., and Wang, X.: The trade-off and synergy between ecosystem services in the Grain-for-Green areas in Northern Shaanxi: China, Ecol. Indic., 43, 103-113, https://doi.org/10.1016/j.ecolind.2014.02.028, 2014.

24. Jin, H., He, R., Cheng, G., Wu, Q., Wang, S., Lü, L., and Chang, X.: Changes in frozen ground in the Source Area of the Yellow River on the QinghaiTibet Plateau, China, their eco-environmental impacts, Environ. Res. Lett., 4(4), 045206, http://doi.org/10.1088/1748-9326/4/4/045206, 2009.

25. Jin, H., Luo, D., Wang, S., Lü, L., and Wu, J.: Spatiotemporal variability of permafrost degradation on the Qinghai-Tibet Plateau, Sci. in Cold and Arid Reg., 3(4), 281-305, 2011.

26. Jin, Z., Guo, L., Yu, Y., Luo, D., Fan, F., and Chu, G.: Storm runoff generation in headwater catchments on the Chinese Loess Plateau after long-term vegetation rehabilitation, Sci. Total Environ., 748, 141375, http://doi.org/10.1016/j.scitotenv.2020.141375, 2020.

27. Li, C., Zhang, Y., Shen, Y., Kong, D., and Zhou, X.: LUCC-Driven Changes in Gross Primary Production and Actual Evapotranspiration in Northern China, J. Geophys. Res.: Atmospheres., 125(6), 13, https://doi.org/10.1029/2019JD031705, 2020.

28. Li, L. and Schwartz, M. D.: Landscape phenology: an integrative approach to seasonal vegetation dynamics, Landscape Ecol., 24(4), 465-472, https://doi.org/10.1007/s10980-009-9328-x, 2009.

29. Liang, W., Bai, D., Wang, F., Fu, B., Yan, J., Wang, S., Yang Y., Long, D., and Feng, M.: Quantifying the impacts of climate change and ecological restoration on streamflow changes based on a Budyko hydrological model in China's loess plateau, Water Resour. Res., 51, 6500-6519, https://doi.org/10.1002/2014WR016589, 2015.

30. Liang, X., Lettenmaie, D. P., Wood, E., and Burges, S. J.: A simple hydrologically based model of land surface water and energy fluxes for general circulation models, J. Geophys. Res. Atmos., 99, 14415-14428, https://doi.org/10.1029/94JD00483, 1994.

31. Liang, X., Wood, E., and Lettenmaier, D. P.: Surface soil moisture parameterization of the VIC-2L model: Evaluation and modification, Glob. Planet Change, 13, 195-206, https://doi.org/10.1016/0921-8181(95)00046-1, 1996.

32. Liu, D., Chen, Y., Cai, W., Dong, W., Xiao, J., Chen, J., Zhang, H., Xia, J., and Yuan, W.: The contribution of China's Grain to Green Program to carbon sequestration, Landsc. Ecol., 29, 1675-1688, https://doi.org/10.1007/s10980-014-0081-4, 2014.

745 33. Liu, J., Zhang, Q., Singh, V. P., and Shi, P.: Contribution of multiple climatic variables and human activities to streamflow changes across China, J. Hydrol., 545, 145-162, http://doi.org/10.1016/j.jhydrol.2016.12.016, 2016.

34. Liu, M., Adam, J. C., Richey, A. S., Zhu, Z., and Myneni, R. B.: Factors controlling changes in evapotranspiration, runoff, and soil moisture over the conterminous U.S: Accounting for vegetation dynamics, J. Hydrol., 565, 123-137, http://doi.org/10.1016/j.jhydrol.2018.07.068, 2018.

750 35. Liu, X. and Gao, Y.: Sediment reduction effects of check dams in the Loess Plateau, Science Press, Beijing, China. (in Chinese), 2020.

36. Liu, X., Gao, Y., and Dang, S.: Evaluation of sediment changes of the Loess Plateau, Yellow River Conservancy Press, Zhengzhou, China. (in Chinese), 2021.

37. Liu, Z., and Liu, Y.: Does Anthropogenic Land Use Change Play a Role in Changes of Precipitation Frequency and

755 Intensity over the Loess Plateau of China? Remote Sens., 10(11), 1818, 2018.

38. Lohmann, D., Nolte-Holube, R., and Raschke, E.: A largescale horizontal routing model to be coupled to land surface parameterization schemes, Tellus, 48A, 708-721, https://doi.org/10.1034/j.1600-0870.1996.t01-3-00009.x, 1996.

39. Lohmann, D., Raschke, E., Nijssen, B., and Lettenmaier, D. P.: Regional scale hydrology: II. Application of the VIC-2L model to the Weser River: Germany, Hydrol. Sci. J., 43(1), 143-158, https://doi.org/10.1080/02626669809492108,

760 1998.

40. Long, D., Pan, Y., Zhou, J., Chen, Y., Hou, X., Hong, Y., Scanlon, B. R., and Longuevergne, L.:Global analysis of spatiotemporal variability in merged total water storage changes using multiple GRACE products and global hydrological models, Remote Sens. Environ., 192, 198-216, http://doi.org/10.1016/j.rse.2017.02.011, 2017.

41. Luan, J., Zhang, Y., Tian, J., Meresa, H. K., and Liu, D.: Coal mining impacts on catchment runoff, J. Hydrol., 589(15),

765 125101, https://doi.org/10.1016/j.jhydrol.2020.125101, 2020.

42. Matheussen, B., Kirschbaum, R. L., Goodman, I. A., O'Donnell, G. M., and Lettenmaier, D. P.: Effects of land cover change on streamflow in the interior Columbia River Basin (USA and Canada), Hydrol. Process, 14(5), 867-885, https://doi.org/10.1002/(SICI)1099-1085(20000415)14:5%3C867::AID-HYP975%3E3.0.CO;2-5, 2000.

43. Maurer, E. P., Wood, A. W., Adam, J. C., Lettenmaier,D. P., and Nijssen, B.: A long-term hydrologically based dataset

770 of land surface fluxes and states for the conterminous United States, -J. Clim., 15, 3237-3251, https://doi.org/10.1175/1520-0442(2002)015,3237:ALTHBD.2.0.CO;2, 2002.

44. Menzel, A., Yuan, Y., Matiu, M., Sparks, T., Scheifinger, H., Gehrig, R., and Estrella, N.: Climate change fingerprints in recent European plant phenology, Glob. Chang Biol., 26, 2599-2612, https://doi.org/10.1111/gcb.15000, 2020.

45. Moriasi, D. N., Arnold, J. G., Liew, M. W. Van., Bingner, R. L., Harmel, R. D., and Veith, T. L.: Model evaluation guidelines for systematic quantification of accuracy in watershed simulations, Trans. ASABE., 50(3), 885-900, https://doi.org/10.13031/2013.23153, 2007.

46. Mu, X., Zhang, L., McVicar, T. R., Chille, B., and Gau, P.: Analysis of the impact of conservation measures on stream flow regime in catchments of the Loess Plateau, China, Hydrol. Process, 21(16), 2124-2134, https://doi.org/10.1002/hyp.6391, 2007.

47. Nijssen, B., O'Donnell, G. M., Lettenmaier, D. P., Lohmann, D., and Wood, E. F.: Predicting the discharge of global rivers, J. Clim., 14(15), 3307-3323, https://doi.org/10.1175/1520-0442(2001)014%3C3307:PTDOGR%3E2.0.CO;2, 2001.

48. Nijssen, B., Schnur, R., and Lettenmaier, D. P.: Global retrospective estimation of soil moisture using the variable infiltration capacity land surface model: 1980-1993, J. Clim., 14(8), 1790-1808, https://doi.org/10.1175/1520-0442(2001)014<1790:GREOSM>2.0.CO;2, 2001.

49. Piao, S., Liu, Q., Chen, A., Janssens, I.. A., Fu, Y., Dai, J., Liu, L., Lian, X., Shen, M., and Zhu, X.: Plant phenology and global climate change: current progresses and challenges, Glob. Chang Biol., 25, 1922-1940, https://doi.org/10.1111/gcb.14619, 2019.

50. Piao, S., Yin, G., Tan, J., Cheng, L., Huang, M., Li, Y., Liu, R., Mao, J., Myneni, R. B., Peng, S., Poulter, B., Shi, X., Xiao, Z., Zeng, N., and Zeng, Z.: Detection and attribution of vegetation greening trend in China over the last 30 years, Glob. Chang Biol., 21(4), 1601-1609, http://doi.org/10.1111/gcb.12795, 2015.

51. Roderick, M. L. and Farquhar, G. D.: A simple framework for relating variations in runoff to variations in climatic conditions and catchment properties, Water Resour. Res., 47, W00G07, https://doi.org/10.1029/2010WR009826, 2011.

52. Shao, R., Zhang, B., Su, T., Long, B., Cheng, L., Xue, Y., and Yang, W.: Estimating the increase in regional evaporative water consumption as a result of vegetation restoration over the loess plateau, J. Geophys. Res.: Atmospheres., 124, https://doi.org/10.1029/2019JD031295, 2019.

53. Shi, X., Wood, A. W., and Lettenmaier, D. P.: How essential is hydrologic model calibration to seasonal streamflow forecasting, J. Hydrometeorol., 9, 1350-1363, https://doi.org/10.1175/2008jhm1001.1, 2008.

54. Sun, W., Song, X., Mu, X., Gao, P., Wang, F., and Zhao, G.: Spatiotemporal vegetation cover variations associated with climate change and ecological restoration in the Loess Plateau, Agric. For. Meteorol., 209-210(1), 87-99, https://doi.org/10.1016/j.agrformet.2015.05.002, 2015.

55. Tang, Q., Oki, T., Kanae, S., and Hu, H.: Hydrological cycles change in the Yellow River basin during the last half of the twentieth century, J. Clim., 21 (8), 1790-1806, https://doi.org/10.1175/2007JCLI1854.1, 2008.

56. Tang, Q., Vivoni, E. R., Muñoz-Arriola. F., and Lettenmaier, D. P.: Predictability of Evapotranspiration Patterns Using Remotely Sensed Vegetation Dynamics during the North American Monsoon, J. Hydrometeorol., 13(1), 103-121, https://doi.org/10.1175/JHM-D-11-032.1, 2012.

57. Tang, Q.: Global change hydrology: Terrestrial water cycle and global change, Sci. China Earth. Sci., 63, 459-462, https://doi.org/10.1007/s11430-019-9559-9, 2020.

58. Tang, Y., Tang, Q., Tian, F., Zhang, Z., and Liu, G.: Responses of natural runoff to recent climatic variations in the Yellow River basin, China, Hydrol. Earth Syst. Sci., 17, 4471-4480, https://doi.org/10.5194/hess-17-4471-2013, 2013.

59. Tesemma, Z. K., Wei, Y., Peel, M. C., and Western, A.: The effect of year-to-year variability of leaf area index on Variable Infiltration Capacity model performance and simulation of runoff, Adv. Water Resour., 83, 310-322, https://doi.org/10.1016/j.advwatres.2015.07.002, 2015.

60. Tian, Y., Li, F., and Liu, P.: Economic analysis of rainwater harvesting and irrigation methods, with an example from China, Agric. Water Manag., 60, 217-226, http://doi.org/10.1016/S0378-3774(02)00171-3, 2003.

61. Todini, E.: The ARNO rainfall-runoff model, J. Hydrol., 175, 339-382, https://doi.org/10.1016/S0022-1694(96)80016-3, 1996.

62. Vivoni, E. R., Moreno, H. A., Mascaro, G., Rodriguez, G. C., Watts, C. J., Payan, J. G., and Russell, L. S.: Observed relation between evapotranspiration and soil moisture in the North American monsoon region, Geophys. Res. Lett., 35(22), https://doi.org/10.1029/2008GL036001, 2008.

63. Wang, G., Zhang, J., and Yang, Q.: Attribution of runoff change for the Xinshui River catchment on the Loess Plateau of China in a changing environment, Water, 8(6), 267, http://doi.org/10.3390/w8060267, 2016.

64. Wang, G., Zhang, J., He, R., Liu, C., Ma, T., Bao, Z., and Liu, Y.: Runoff sensitivity to climate change for hydro-climatically different catchments in China, Stoch. Environ. Res. Risk Assess., 31(4):1011-1021, https://doi.org/10.1007/s00477-016-1218-6, 2017.

65. Wang, G., Zhang, J., Jin, J., Pagano, T. C., Calow, R., Bao, Z., Liu, C., Liu, Y., and Yan, X.: Assessing water resources in China using PRECIS projections and a VIC model, Hydrol. Earth Syst. Sci., 16, 231–240, https://doi.org/10.5194/hess-16-231-2012, 2012.

66. Wang, Y., Shao, M., Zhu, Y., and Liu, Z.: Impacts of land use and plant characteristics on dried soil layers in different climatic regions on the Loess Plateau of China. Agric. For. Meteorol., 151(4), 437-448, https://doi.org/10.1016/j.agrformet.2010.11.016, 2011.

67. Wang, Y., Wang, S., Wang, C., and Zhao, W.: Runoff sensitivity increases with land use/cover change contributing to runoff decline across the middle reaches of the Yellow River basin, J. Hydrol., 600: 126536, https://doi.org/10.1016/j.jhydrol.2021.126536, 2021.

68. Wang, Z., Cui, Z., He, T., Tang, Q., Xiao P., Zhang, P., and Wang, L.: Attributing the Evapotranspiration Trend in the Upper and Middle Reaches of Yellow River Basin Using Global Evapotranspiration Products, Remote Sens., 14(1), 175, http://doi.org/10.3390/rs14010175, 2022.

69. Wang, Z., Yao W., Tang, Q., Liu, L., Xiao, P., Kong, X., Zhang, P., Shi, F., and Wang, Y.:Continuous Change Detection of Forest/Grassland and Cropland in the Loess Plateau of China Using All Available Landsat Data, Remote Sens., 10, 1775,https://doi.org/10.3390/rs10111775, 2018.

70. Wu, C., Hou, X., Peng, D., Alemu, G., and Xu, S.: Land surface phenology of China's temperate ecosystems over1999-2013: Spatial-temporal patterns, interaction effects, covariation with climate and implications for productivity, Agric. For. Meteorol., 216, 177-187, https://doi.org/10.1016/j.agrformet.2016.01.087, 2016.

71. Wu, J., Miao, C., Zhang, X., Yang, T., and Duan, Q.: Detecting the quantitative hydrological response to changes in climate and human activities, Sci. Total Environ., 586, 328-337, http://doi.org/10.1016/j.scitotenv.2017.02.010, 2017.

72. Wu, J., Wang, Z., Dong, Z., Tang, Q., Lv, X., and Dong, G.: Analysis of Natural Streamflow Variation and Its Influential Factors on the Yellow River from 1957 to 2010, Water, 10(9):1155, https://doi.org/10.3390/w10091155, 2018

73. Wu, Q. and Zhang, T.: Recent permafrost warming on the Qinghai-Tibetan Plateau, J. Geophys. Res. Atmos., 113, D13108, http://doi.org/10.1029/2007JD009539, 2008.

74. Wu, Z., Chen, S., De Boeck, H. J., Stenseth, N. C., Tang, J., Vitasse, Y., and Morellato, P.: Atmospheric brightening counteracts warming-induced delays in autumn phenology of temperate trees in Europe, Glob. Ecol. Biogeogr., 30(12), 2477-2487, https://doi.org/10.1111/geb.13404, 2012.

75. Xiao, Z., Liang, S., Wang, J., Chen, P. Yin, X., Zhang, L., and Song, J.: Use of general regression neural networks for generating the GLASS leaf area index product from time-series MODIS surface reflectance, IEEE Trans. Geosci. Remote Sens., 52, 209-223., https://doi.org/10.1109/TGRS.2013.2237780, 2014.

76. Xie, H., Xie, Z., Yuan, Q., Duan, Q., Zheng, X., Liang, X., Chen, G., and Guo, F.: Regional parameter estimation of the VIC land surface model: methodology and application to river basins in China, J. Hydrometeorol., 8(3), 447-468, http://doi.org/10.1175/JHM568.1, 2007.

77. Xie, X., Liang, S., Yao, Y., Jia, K., Meng, S., and Li, J.: Detection and attribution of changes in hydrological cycle over the Three-North region of China: Climate change versus afforestation effect, Agric. For. Meteorol., 203 74-87, https://doi.org/10.1016/j.agrformet.2015.01.003, 2015

78. Xu, Z., Li, J., and Liu, C.: Long-term trend analysis for major climate variables in the Yellow River Basin, Hydrol. Process, 21, 1935-1948, https://doi.org/10.1002/hyp.6405, 2007.

79. Yang, S., Kang, T., Bu, J., Chen, J., and Gao, Y.: Evaluating the Impacts of Climate Change and Vegetation Restoration on the Hydrological Cycle over the Loess Plateau, China, Water, 11(11):2241, https://doi.org/10.3390/w11112241, 2019.

80. Yang, W., Chen, H., Xu, C., Huo, R., Chen, J., and Guo, S.: Temporal and spatial transferabilities of hydrological models under different climates and underlying surface conditions, J. Hydro., 591:125276, https://doi.org/10.1002/hyp.6405, 2020.

81. Yao, W., Xu, J., and Ran, D.: Evaluation of water and sediment changes of the Yellow River Basin, The Yellow River Water Conservancy Press, Zhenzhou, Henan (in Chinese), 2011.

82. Yao, Y., Xie, X., Meng, S., Zhu, B., Zhang, K., and Wang, Y.: Extended Dependence of the Hydrological Regime on the Land Cover Change in the Three-North Region of China: An Evaluation under Future Climate Conditions, Remote Sens., 11(1), 81, https://doi.org/10.3390/rs11010081, 2019.

83. Yapo, P., Gupta, H. V., and Sorooshian, S.: Multi-objective global optimization for hydrologic models, J. Hydrol., 204, 83-97, https://doi.org/10.1016/S0022-1694(97)00107-8, 1998.

84. Yuan, X., Ma, F., Wang, L., Zheng, Z., Ma, Z., Ye, A., and Peng, S.: An experimental seasonal hydrological forecasting system over the Yellow River basin-Part 1: understanding the role of initial hydrological conditions, Hydrol. Earth Syst. Sci., 20, 5477-5492, https://doi.org/10.5194/hess-20-2437-2016, 2016.

85. Yuan, X., Zhang, M., Wang, L., and Zhou, T.: Understanding and seasonal forecasting of hydrological drought in the Anthropocene, Hydrol. Earth Syst. Sci., 21, 5477-5492, https://doi.org/10.5194/hess-21-5477-2017, 2017.

86. Zhai, R. and Tao, F.: Climate change in China affects runoff and terrestrial ecosystem water retention more than changes in leaf area index and land use/cover over the period 1982–2015, J. Geophys. Res. Biogeosci., 126, e2020JG005902, https://doi.org/10.1029/2020JG005902, 2021.

87. Zhai, R., Tao, F., and Xu, Z.: Spatial-temporal changes in runoff and terrestrial ecosystem water retention under 1.5 and 2°C warming scenarios across China, Earth Syst. Dyn., 9(2), 717-738, http://doi.org/10.5194/esd-9-717-2018, 2018.

88. Zhang, S., Yang, D., Yang, Y., Piao, S., Yang, H., Lei, H., and Fu, B.: Excessive afforestation and soil drying on China's Loess Plateau, J. Geophys. Res.: Biogeosciences., 123, https://doi.org/10.1002/ 2017JG004038, 2018.

89. Zhang, S., Yang, H., Yang, D., and Jayawardena, A. W.: Quantifying the effect of vegetation change on the regional water balance within the Budyko framework, Geophys. Res. Lett., 43, 1140-1148. https://doi.org/10.1002/2015GL066952, 2016.

90. Zhang, X., Liu, L., Chen, X., Gao, Y., Xie, S., and Mi, J.: GLC_FCS30: Global land-cover product with fine classification system at 30 m using time-series Landsat imagery, Earth Syst. Sci. Data, 13, 2753-2776, https://doi.org/10.5194/essd-2020-182, 2021.

91. Zhang, X., Tang, Q., Pan, M., and Tang, Y.: A Long-Term Land Surface Hydrologic Fluxes and States Dataset for China, J. Hydrometeorol., 15, 2067-2084, http://doi.org/10.1175/JHM-D-13-0170.1, 2014.

92. Zhang, X., Zhang, L., Zhao, J., Rustomji, P., and Hairsine, P.: Responses of streamflow to changes in climate and land use/cover in the Loess Plateau, China, Water Resour. Res., https://doi.org/10.1029/2007WR006711, 2008.

93. Zhang, Y., Peng, C., Li, W., Tian, L., Zhu, Q., Chen, H., Fang, X., Zhang, G., Liu, G., Mu, X., Li, Z., Li, S., Yang, Y., Wang, J., and Xiao, X., Multiple afforestation programs accelerate the greenness in the 'Three North' region of China from 1982 to 2013, Ecol. Indic., 61, 404-412, https://doi.org/10.1016/j.ecolind.2015.09.041, 2016.

94. Zhang, Z., Chen, X., Xu, X., Yuan, L., Yong, B., and Yan, S.: Evaluating the non-stationary relationship between precipitation and streamflow in nine major basins of China during the past 50 years, J. Hydrol., 409 (1-2): 81-93, https://doi.org/10.1016/j.jhydrol.2011.07.041, 2011.

95. Zhao, G., Li, E., Mu, X., Wen, Z., Rayburg, S., and Tian, P.: Changing trends and regime shift of streamflow in the Yellow River basin., Stoch. Environ. Res. Risk Assess., https://doi.org/10.1007/s00477-015-1058-9, 2015.

96. Zhao, G., Tian, P., Mu, X., Jiao, J., Wang, F., and Gao, P.: Quantifying the impact of climate variability and human activities on streamflow in the middle reaches of the Yellow River basin, China, J. Hydrol., 519, 387-398, https://doi.org/10.1016/j.jhydrol.2014.07.014, 2014.

97. Zhu, B., Xie, X., Lu, C., Lei, T., Wang, Y., Jia, K., and Yao, Y.: Extensive Evaluation of a Continental-Scale High-Resolution Hydrological Model Using Remote Sensing and Ground-Based Observations, Remote Sens., 13(7), 1247, https://doi.org/10.3390/rs13071247, 2021.

98. Zhu, Z., Piao, S., Myneni, R. B., Huang, M., Zeng, Z., Canadell, J. G., Ciais, P., Sitch, S., Friedlingstein, P., Arneth, A., Cao, C., Cheng, L., Kato, E., Koven, C., Li, Y., Lian, X., Liu, Y., Liu, R., Mao, J., Pan, Y., Peng, S., Peñuelas, J., Poulter, B., Pugh, T. A. M., Stocker, B. D., Viovy, N., Wang, X., Wang, Y., Xiao, Z., Yang, H., Zaehle, S., and Zeng, N.: Greening of the Earth and its drivers, Nat. Clim. Chang, 6(8), 791-795, http://doi.org/10.1038/nclimate3004, 2016.